17 Adhesion and Wetting Phenomena

17.1 Surface and Interfacial Energies

In Part I we saw how various interaction potentials between molecules arise, and we considered the implications of the energy minimum, or the "adhesion" energy, of molecules in contact. Here we shall look at phenomena involving particles and extended surfaces in adhesive contact, and it is best to begin by defining some commonly used terms and deriving some useful thermodynamic relations.

Work of adhesion and cohesion in a vacuum. These are the free energy changes, or reversible work done, to separate unit areas of two surfaces or media from contact to infinity in a vacuum (Figure 17.1a, b). For two different media ($1 \neq 2$), this energy is referred to as the work of adhesion W_{12}, while for two identical media ($1 = 2$), it becomes the work of cohesion W_{11}. If 1 is a solid and 2 a liquid, W_{12} is often denoted by W_{SL}. Note that since all media attract each other in a vacuum W_{11} and W_{12} are always positive—that is, of opposite sign to the reverse processes of bringing surfaces *into* contact from infinity (See footnote 2 in Chapter 10).

Surface energy, surface tension. This is the free energy change γ when the surface area of a medium is increased by unit area. Now the process of creating unit area of surface is equivalent to separating two half-unit areas from contact (Figure 17.1b, c), so that we may write

$$\gamma_1 = \frac{1}{2} W_{11}. \tag{17.1}$$

For solids γ_1 is commonly denoted by γ_s and is given in units of energy per unit area: mJ m^{-2} (the same as erg/cm^2). For liquids, γ_1 is commonly denoted by γ_L and is usually given in units of tension per unit length: mN m^{-1} (the same as dyn/cm), which is numerically and dimensionally the same as the surface free energy.

It is evident that the intermolecular forces that determine the surface energy of a substance are the same as those that determine its latent heat and boiling point (Section 2.6). As might be expected, substances such as metals with high boiling points ($T_B > 2000°C$) usually have high surface energies ($\gamma > 1000$ mJ m^{-2}), while lower boiling point substances have progressively lower surface energies. For example, for mercury: $\gamma = 485$ mJ m^{-2}, $T_B = 357°C$; for water: $\gamma = 73$ mJ m^{-2}, $T_B = 100°C$; for argon: $\gamma = 13.2$ mJ m^{-2}, $T_B = -186°C$; and for hydrogen: $\gamma = 2.3$ mJ m^{-2}, $T_B = -253°C$. In Section 13.13 we saw how the surface energies of all but strongly polar or H-bonding liquids and solids can be calculated reasonably accurately on the basis of current theories of van der Waals forces. Additional short-range forces that contribute to surface energies and adhesion are metallic bonds (Section 13.14) and charge exchange (including acid-base) interactions

Intermolecular and Surface Forces. 3rd edition, DOI: 10.1016/B978-0-12-391927-4.10017-9
Copyright © 2011, Elsevier Inc. All rights reserved.

quantitative and qualitative differences. These include the definitions of the radii of curvature and areas per molecule, the resulting deformations when molecules are drawn into the bulk, and the different effects of cooperative (nonadditive) interactions. For example, in the case of the 13-atom cluster (Figure 17.4), each surface atom has 7 open bonds and there are therefore $12 \times 7 = 84$ of them, which must be the same as for the complementary hole. But while having the same total surface energy, the radii of the clusters and holes, R_{drop} and R_{hole}, are different when defined in terms of their outer and inner boundaries. Thus, in Figure 17.4, $R_{\text{drop}} = 3a$ but R_{hole} is smaller and given by $R_{\text{hole}} = (4\sqrt{2/3} - 1)a = 2.27a$, so that the surface energy of the hole is

$$\gamma \approx 7 \times 12w/2[4\pi(2.27a)^2] \approx 0.65w/a^2 \text{ J m}^{-2} \qquad \text{for a 13-atom hole,} \qquad (17.13)$$

which is greater than the surface energies of both the planar surface, Eq. (17.9), and the 13-atom cluster or drop, Eq. (17.11).

These differences in the surface energies of droplets and holes are partly due to the somewhat arbitrary definition of their radii (not to mention that small clusters are not even spherical). A more consistent definition of radius would be that of the sphere whose surface passes through the contact points—the effective bond centers defined by R_{bonds} in Figure 17.4—between the outermost spheres and the next layer of spheres. This would give the same radius for complementary spheres and holes. When this is done for the 13-atom cluster one obtains $R_{\text{drop}} = R_{\text{hole}} = \sqrt{19/3}a = 2.52a$, which is intermediate between $3.0a$ and $2.27a$, as expected. With this common radius, the surface energies of the 13-atom cluster and hole are now the same:

$$\gamma \approx 7 \times 12w/2[4\pi(2.52a)^2] \approx 0.53w/a^2 \qquad \text{for a 13-atom cluster or hole,} \qquad (17.14)$$

which is 23% higher than the value for a planar surface, Eq. (17.9). A higher value was also obtained for a single atom, Eq. (17.10). The problem of exactly where to define the boundaries of small particles comes up when considering other properties that involve their radius, length, area, or volume—for example, the strain, stress, defining the Young's modulus, and so on.

Worked Example 17.2

Question: A single 13-molecule cluster of medium 1 resides in a liquid medium 2. What is the effective interfacial energy of the cluster in terms of the bulk surface energy γ_i? What is it in the case of a single molecule of 1 in medium 2? Assume that both types of molecules have the same radius a, and that the pair contact energies are $-w_{11}$, $-w_{22}$, and $-w_{12}$, Discuss the implications of your results.

Answer: Following the method of calculating of the surface energy of a single surface in Section 13.13, the interfacial energy of the planar interface is $\gamma_i(\infty) \approx \frac{3}{2}\left(\frac{w_{11} + w_{22} - 2w_{12}}{\sigma^2 \sin 60^\circ}\right) = 0.43(w_{11} + w_{22} - 2w_{12})/a^2$. For a cluster of one material coexisting in another, the concept of a different outer and inner radius, as arises for isolated clusters and cavities, becomes

untenable. The common radius will be defined as the locus of the contact points or bonds, which occurs at $R = 2.52a$ for the 13-molecule cluster and at $R = a$ for the single molecule. The total change in energy per cluster can be determined by calculating the energy change of transferring the cluster from medium 2 into its own bulk medium 1, since this eliminates the interface which defines the reference state of zero energy. The transfer process is similar to the four-step process of Figure 17.1g involving a change in energy of $\Delta w = (w_{12} - \frac{1}{2}w_{22} + \frac{1}{2}w_{11} - w_{11}) = -\frac{1}{2}(w_{11} + w_{22} - 2w_{12})$ per bond at the interface. Since there are $5 \times 7 = 84$ such bonds at the 13-cluster interface, the interfacial energy is therefore $\gamma_i(R = 2.52a) \approx 84\ (w_{11} + w_{22} - 2w_{12})/2[4\pi(2.52a)^2] \approx 0.53\ (w_{11} + w_{22} - 2w_{12})/a^2 = 1.23\gamma_i(\infty)$. Applying the same argument to the single molecule "cluster" we obtain for its interfacial energy: $\gamma_i(R = a) \approx 12\ (w_{11} + w_{22} - 2w_{12})/2(4\pi a^2) = 1.1\ \gamma_i(\infty)$. The effect is therefore the same as for the surface tension—that is, resulting in an increased interfacial energy. The result is also unchanged on exchanging media 1 and 2. This trend arises because at a curved interface, whether concave or convex, there are always more higher energy 1-2 or 2-1 bonds than at the planar interface. Since the interfacial energy is positive—that is, unfavorable—the surfaces of smaller droplets tend to evaporate or dissolve faster than larger droplets.

■ ■ ■

Still, it is clear that for pair-wise additive interactions the surface energies per unit area of even the smallest nano-droplets and cavities are already very close to those of the planar surfaces and that any difference really depends on how their radii are defined. Thus, describing particles, whether ordered or amorphous, in terms of their radii can be confusing. It is also unnecessary. It is far better to analyze the energetics of clusters in terms of the energy *per molecule*—that is, to define clusters in terms of the number of molecules in the cluster rather than the radius of the cluster. Molecular and molar energies also enter naturally into basic equations of thermodynamics and statistical mechanics, whereas radii do not (see later sections on self-assembly and nucleation in Part III).

When expressed in terms of the energies per molecule, the picture changes completely: the 84 surface bonds of the 13-molecule cluster are shared with 42 molecules in the next layer. Thus, while per unit area the cluster and hole energies are similar, when reckoned *per surface molecule* the cluster energies are $42/12w = 3.5w$ per molecule and the hole energies are $42/42w = 1.0w$ per molecule, a difference of 350%. The differences are also large, especially for the cavity, when compared to the energies of the planar surfaces of $3.0w$ per molecule. This may be readily understood by considering that the molecules on a convex surface have fewer bonds, while those on concave surfaces have more bonds than those on planar surfaces. In the case of a single molecule, the cluster and hole energies are $6.0w$ (cf. Eq. 2.3) and $6w/12 = 0.5w$, respectively. The hole energy is now very small because each surface molecule is surrounded by 11 other molecules, making it effectively in the bulk state—the reference state of zero energy. Due to the much lower number of cohesive bonds holding molecules and small clusters, these are often in a different phase state from the bulk material. Thus small gold particles are liquid at temperatures where the bulk metal is solid (see below), and small volumes of liquid may have a density intermediate between the vapor and (bulk) liquid phase (Stroud et al., 2001).

The nanoparticle regime. The analysis so far has assumed that atoms and small molecules interact via additive pair potentials where long-range forces and many-body effects are not important. While this condition holds for van der Waals solids and liquids, it does not apply to metallic, semiconducting, ionic, and hydrogen-bonding compounds, where a certain number of atoms are needed for some property to reach the saturation or bulk value.

In Chapter 11, particularly Section 11.4, we considered how size affects the nonadditive properties of particles as they grow from single atoms to macroscopic bodies exhibiting bulk properties. For example, the high latent heats, melting points, surface energies, electronic and optical properties of metals, and semiconductors depend on the correlated (cooperative) interactions of many atoms. In very small droplets or ultrathin films these medium- to long-range correlations cannot occur, and some metal clusters with less than 15–30 atoms lose many of their bulk metallic properties and become indistinguishable from van der Waals substances. For example, the melting points of small droplets of gold are significantly lower than the bulk value of 1336 K, falling to 1000 K for a cluster of diameter 4 nm and to about 500 K for a diameter of 2.5 nm (Buffat and Borel, 1976). Similarly, Buffey and colleagues (1990) have found that small water clusters with about 20 molecules or less are probably in the liquid state already at 200 K due to the inability of a H-bonding network to develop in these clusters. A related effect occurs with thin water films: thus, between 0 and −20°C the surface of ice has a thin liquid layer on it—a phenomenon known as "surface melting"—which is responsible for the low friction of ice (Dash, 1989).

Thus, the different properties of clusters and nanoparticles are not so much to do with their size or curvature effects per se but on the reduced number of bonds at surfaces (even flat surfaces as in the case of the low friction of ice) and/or on the nonadditive (cooperative) intermolecular interactions. Further aspects of these "skin effects" and "proximity effects" were discussed in Section 11.4, and the role of nonequilibrium interactions in their assembly is discussed in Chapter 22 in Section 22.7 on self-assembly versus directed assembly.

The Laplace pressure. For surfaces with large, macroscopic radii, curvature effects are still important, since they give rise to a significant *Laplace pressure* P_L within the liquid or solid. Returning to Figure 17.5, the surface tension force of γ per unit length, when resolved normal to a circumferential circle of radius R gives a net force of $F = 2\pi R\gamma$ that acts to compress the droplet and that at equilibrium must be balanced by an internal pressure given by P = net force/area $= 2\pi R\gamma/\pi R^2 = 2\gamma/R$. More generally, for a surface with two orthogonal or "principal" radii, R_1 and R_2:

$$P_L = \gamma(1/R_1 + 1/R_2). \tag{17.15}$$

Thus, for a spherical droplet or hole of radius R we obtain the above result, $P_L = 2\gamma/R$, while for a cylinder of radius R, $P_L = \gamma/R$.

The convention of defining the meniscus curvature relative to the condensed phase—for example, positive for liquid droplet but negative for a hole—can cause confusion

regarding the sign or direction of the pressure. It is best to remember that the Laplace pressure always drives the interface *in the concave direction*. Thus, the liquid in a drop (convex surface) experiences a positive (compressive) pressure, whereas a liquid containing a bubble or hole (concave surface) experiences a negative (tensile) pressure. The positive Laplace pressure on a droplet means that its molecules are compressed – much like the stretched elastic membrane of a balloon compresses the gas inside it, while around a concave surface the molecules are expanded, such as when liquid rises up a capillary tube or when a liquid droplet spreads between two sheets pulling them together (see Section 17.11 on capillary forces). This issue becomes most clearly apparent when we try to establish whether the pressure inside a liquid droplet immersed in another liquid is positive or negative: it is always positive since γ_i is always positive[2] (Section 17.1).

Worked Example 17.3

Question: Can the Laplace pressure be applied to curved surfaces having molecular dimensions?
Answer: Consider the limit of just two molecules in adhesive contact for which the "internal" Laplace pressure would be given by $P = 2\gamma/a$, where $\sigma = 2a$. In terms of molecular parameters, where the molecular contact area is $\sim\pi a^2$. Using Eq. (17.9) this pressure corresponds to a "Laplace force" of $f_{Lap} \approx 2[\sqrt{3}w(\sigma)/4a^2]\pi a^2/a = 2.7w(\sigma)/a$. Assuming a van der Waals pair potential of $w(r) = -C/r^6$ with a hard-wall cut-off at $r = \sigma$, the van der Waals adhesion force is $f(\sigma) = -6C/\sigma^7 = 6w(\sigma)/\sigma = 3.0w(\sigma)/a$. The Laplace and intermolecular forces are therefore calculated to be within 10% of each other. The concept and quantitative application of the Laplace pressure therefore appears to apply to molecular clusters including dimers, where it is seen to reduce to none other than the pair-interaction between two molecules.

Worked Example 17.3 shows that the Laplace pressure can be enormous, enough to make liquids rise many tens of meters in fine capillary tubes and to the tops of tall trees.[3] For van der Waals liquids where, typically, $\gamma \approx 30$ mJ m^{-2}, for $R = a = 0.3$ nm, pressures as high as $2(30 \times 10^{-3})/(3 \times 10^{-10}) = 2 \times 10^8$ Pa $\approx$ 2,000 atm can therefore be attained. Situations where such highly curved (concave) menisci and high local pressures arise occur at cracks and contact boundaries—for example, between surfaces or their asperities. A liquid does not have to be present at such boundaries: the equation for the Laplace pressure applies equally to solids and liquids, and for solids where γ is usually much higher than for liquids the pressure will be correspondingly higher.

[2]The two liquids must be immiscible or partially miscible. A negative γ_i means that the droplet will eventually dissolve in the host liquid—in other words, that the interface will disappear, since it wants to *increase* its area.

[3]An analogous situation arises with gravitational pressure: in a star of mass M and radius R the compressive pressure at the center can be readily shown (by considering the pressure between two hemispheres) to be approximately $GM^2/4\pi R^4 \propto R^2$. However, due to the long-range nature of gravitational forces this pressure is not uniform but is highest at the center. It also increases rather than decreases with R, and can lead to the gravitational collapse of large stars into neutron stars with radii as small as 10 km.

There is one important fundamental difference between convex and concave surfaces, which concerns the thermodynamic equilibrium state of these surfaces. As shown in Section 17.11, a planar or concave surface can be stable in saturated or undersaturated vapor, respectively, but a convex surface is only metastable in oversaturated vapor. Oversaturated vapor spontaneously condenses until the vapor pressure reaches or falls below the saturated pressure and the liquid-vapor interface is planar, becomes concave or disappears (as when a hole closes up).

Worked Example 17.4

Question: A hollow cylindrical straw has two macroscopic soap bubbles of different radii, R_1 and R_2, where $R_1 < R_2$, at each end. Air can flow freely between the bubbles through the straw, and their Laplace pressure is given by $P_L = 2\gamma/R_i$, where $\gamma = \text{const}$. No air flows through the soap films. What is the final stable configuration of the system?

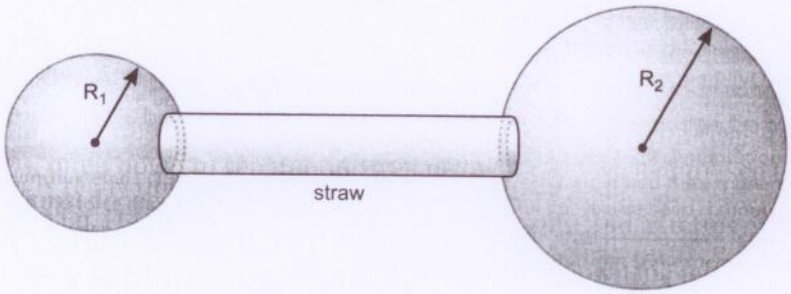

Answer: The Laplace pressure difference will drive air from the smaller bubble to the larger one until the pressure has equilibrated throughout the system. This will occur when both bubbles have the same radius, R. The initially larger bubble will have grown and the initially smaller bubble will have shrunk, first to where its radius equals that of the straw diameter, then further—but now with *increasing* radius—to the point where it exists as a slightly convex bulge at the circular opening of the straw. Since both truncated "bubbles" have the same radius R and truncated contact area with the straw, they are geometrically complementary parts of a complete sphere of radius R. Assuming that the total internal volume (of the air and, therefore, bubbles) has not changed, the radius of the two end "bubbles" will therefore be given by $R^3 = R_1^3 + R_2^3$. In practice, if the gas is ideal, will R be larger or smaller?

17.4 Contact Angles and Wetting Films

Surface and interfacial energies determine how macroscopic liquid droplets deform when they adhere to a surface. In Figure 17.6a (top) a large initially spherical droplet 2 in medium 3 approaches and then settles on the rigid flat surface of medium 1. The final total surface energy of the system is therefore given by

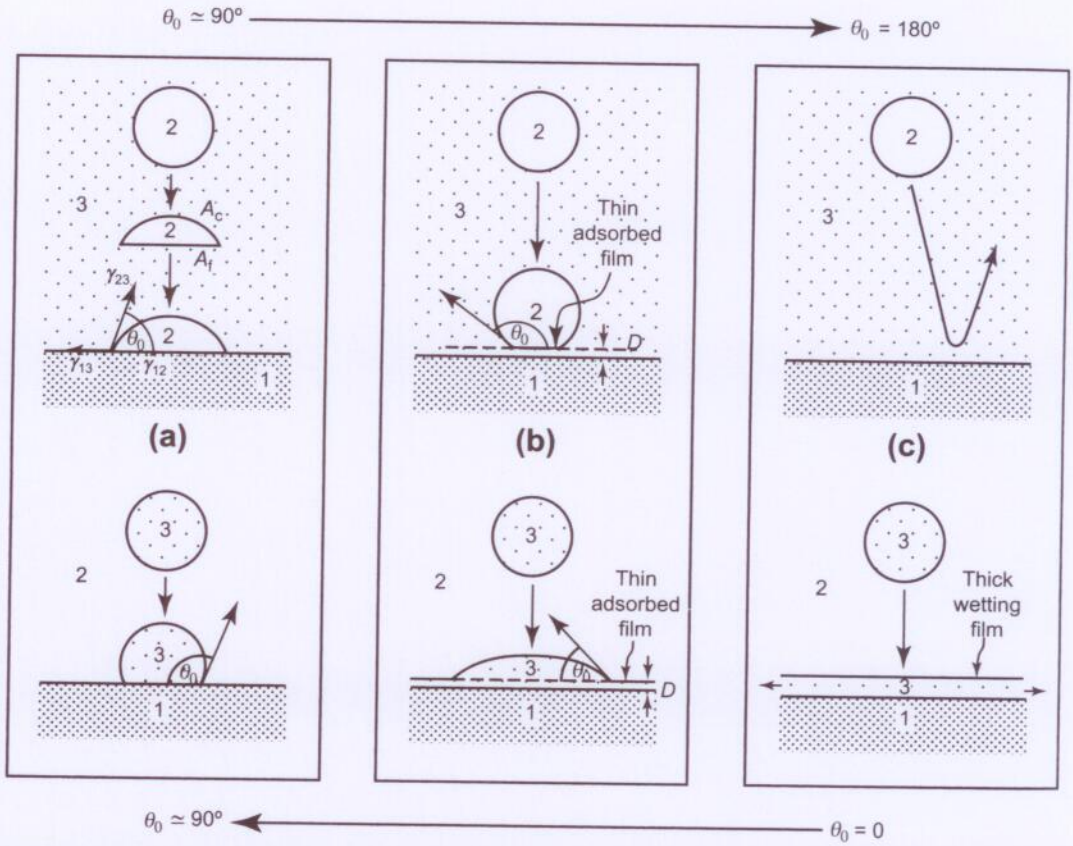

FIGURE 17.6 Contact angles and their manifestation from $\theta = 0$ to $\theta = 180°$. Note that the upper and lower drawings in each box are formally equivalent on interchanging media 2 and 3 and replacing θ_0 by $(180° - \theta_0)$. The thin adsorbed films in the middle panel are an example of "autophobicity"—the nonwetting of a liquid on a layer of itself. Such films can be molecularly thin with "quantized" thicknesses. For a spreading droplet on a surface they are referred to as precursor films.

$$W_{\text{tot}} = \gamma_{23}(A_c + A_f) - W_{132}A_f, \tag{17.16}$$

where A_c and A_f are the curved and flat areas of the droplet. At equilibrium: $\gamma_{23}(dA_c + dA_f) - W_{132}dA_f = 0$. For a droplet of constant volume, it is easy to show using straightforward geometry that $dA_c/dA_f = \cos\theta$. Thus, the equilibrium condition ($\theta = \theta_0$) is

$$\gamma_{23}(1 + \cos\theta_0) = W_{132} = \gamma_{13} + \gamma_{23} - \gamma_{12}, \tag{17.17}$$

or

$$\gamma_{12} + \gamma_{23}\cos\theta = \gamma_{13}, \tag{17.18}$$

which can also be derived by balancing the resolved interfacial tensions in the plane of the surface (Figure 17.6a).

It is also interesting to resolve the forces normal to the surface: if r is the radius of the contact circle, the net vertically resolved interfacial tension force acting at the rim of the droplet is $2\pi r\gamma_{23}\sin\theta_0$. This should be balanced by the Laplace pressure acting downward on the surface, which is given by $2\gamma_{23}/R$, where R and r are geometrically related by $r = R\sin\theta_0$. The net force due to the Laplace pressure is therefore $2\gamma_{23} \times$ contact area/$R = 2\pi r^2\gamma_{23}/R = 2\pi r\gamma_{23}\sin\theta_0$, which exactly balances the upwardly resolved surface tension force.

If media 2 and 3 are interchanged, as in Figure 17.6a (bottom), then Eq. (17.17) becomes

$$\gamma_{23}(1+\cos\theta_0) = W_{123} = \gamma_{12}+\gamma_{23}-\gamma_{13}, \tag{17.19}$$

that is,

$$\gamma_{12}-\gamma_{23}\cos\theta_0 = \gamma_{13}, \tag{17.20}$$

or

$$\gamma_{23}(1-\cos\theta_0) = W_{132}, \tag{17.21}$$

which is the same as Eq. (17.17) with θ_0 replaced by $180^\circ - \theta_0$. Thus, as might have been expected intuitively, the contact angle in Figure 17.6a (bottom) is simply $180^\circ - \theta_0$ of that in Figure 17.6a (top).[4]

The total "wetting" or "spreading" energy of the droplet on the surface is given by inserting the equilibrium condition, Eq. (17.17), into Eq. (17.16), giving $W_{\text{total}} = W_{\min} = \gamma_{23}(A_c + A_f) - W_{132}A_f = [(A_c + A_f)/(1+\cos\theta_0) - A_f]W_{132} = (A_c - A_f\cos\theta_0)W_{132}/(1+\cos\theta_0)$. The minimum total energy can be expressed more conveniently in terms of the equilibrium contact angle θ_0 and initial radius of the spherical droplet, R_0 (Figure 17.6a):

$$W_{\text{total}} = W_{\min} = 4^{2/3}\pi R_0^2 W_{132}(2-3\cos\theta_0+\cos^3\theta_0)^{1/3}/(1+\cos\theta_0) \tag{17.22a}$$

$$= 4^{2/3}\pi R_0^2\,\gamma_{23}(2-3\cos\theta_0+\cos^3\theta_0)^{1/3} \tag{17.22b}$$

$$= 4\pi R_0^3\,\gamma_{23}/R. \tag{17.22c}$$

Thus, $W_{\min}$ is a maximum for $\theta_0 = 180^\circ$, when $\cos\theta_0 = -1$, $W_{132} = 0$, $R = R_0$, and the energy remains unchanged from the original value of $4\pi R_0^2\,\gamma_{23}$ because there is no adhesion and therefore no adhesive flattening. The total energy of Eq. (17.22) decreases monotonically from $4\pi R_0^2\,\gamma_{23}$ to zero as the contact angle decreases from 180° to zero (i.e., as the droplet spreads on the surface), and as R increases from R_0 to ∞ (i.e., as the Laplace pressure falls to zero). Thus, given a choice, a liquid prefers to wet the surface on which it has the lowest contact angle. As a corollary to this, if a (smooth) surface has

[4]By convention, the contact angle is always the angle measured within the liquid (not vapor) medium. For a liquid-liquid interface—that is, a liquid droplet in another liquid—there is no convention and one needs to specify the liquid within which the angle is defined.

a gradient in its chemical properties such that the contact angle of a particular liquid also varies on it, a droplet of this liquid placed on the surface will move to the region where it subtends the lowest contact angle. This qualitative conclusion could also have been arrived at, more or less immediately, by considering where the Laplace pressure within the droplet is least.

While the above results were derived for the specific case of a spherically shaped droplet on a flat surface, the contact angle is independent of the surface geometry (Adamson, 1976, Chapter 7). Thus, θ_0 is the same on a curved surface, inside a capillary, or at any point on an irregularly shaped surface. Further, the contact angle θ_0 as given by the above equations is a thermodynamic and thus a purely macroscopic, quantity—independent of the nature of the forces between the molecules as long as these are of shorter range than the dimensions of the droplet. Thus, the contact angle tells us nothing about the microscopic contact angle or the shape of the liquid profile at the point where it meets the surface (Figure 17.7).

The above equations are more generalized forms of the famous equations of Young and Dupré derived for liquid droplets on surfaces exposed to vapor. Thus, if medium 3 in Figure 17.6a (top) is an inert atmosphere, Eqs. (17.17) and (17.18) become the Young-Dupré equation:

$$\gamma_2(1 + \cos\theta_0) = W_{12} \tag{17.23}$$

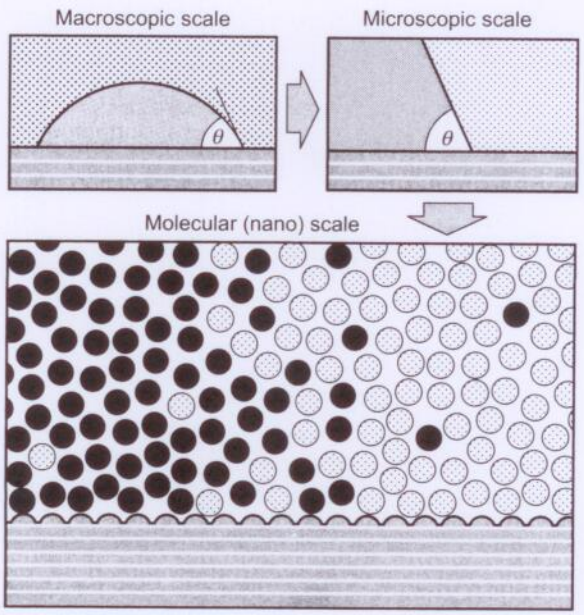

FIGURE 17.7 Schematic shape of a liquid-liquid interface as it meets a solid surface seen at the macroscopic, microscopic and molecular (nanoscopic) levels. The macroscopic contact angle, θ, does not tell us much about the shape of the interface at the molecular level.

and the Young equation:

$$\gamma_{12} + \gamma_2 \cos\theta_0 = \gamma_1. \tag{17.24}$$

For example, for water on paraffin wax, the measured values are $\theta_0 \approx 111°$, γ_1(paraffin) = 25 mJ m^{-2}, and γ_2(water) = 73 mJ m^{-2}, from which we infer that $\gamma_{12} \approx 51$ mJ m^{-2} (cf. Table 17.1) and that $W_{12} \approx 47$ mJ m^{-2}. Note that this is close to the value expected from $W_{12} \approx 2\sqrt{\gamma_1^d \gamma_2^d} \approx 2\sqrt{25 \times 20} \approx 45$ mJ m^{-2}. In some studies all four parameters of the Young equation were independently measured (Pashley and Israelachvili, 1981; Israelachvili, 1982): This involved a droplet of 8×10^{-4} M HTAB surfactant solution on a monolayer-covered surface of mica for which γ_1(solid) = 27 ± 2 mJ m^{-2}, γ_2(liquid) = 40 mJ m^{-2}, γ_{12}(solid-liquid) = 11 ± 2 mJ m^{-2}, and $\theta_0 = 64°$, which agree with the Young equation.

In the case where medium 3 is a liquid, equilibrium can be attained at some finite distance D [Figure 17.6b (top)] where the interaction energy W_{132} is a minimum—for example, a weak secondary minimum (Section 14.21). In such cases the contact angle is usually very low. Such phenomena occur, for example, when dissolved air bubbles or oil droplets containing lipid or surfactant monolayers (emulsion droplets) adhere weakly to each other or to a surface (Figure 1.3d).

An analogous situation occurs when a liquid droplet attaches to a surface containing a thin physisorbed film of the same liquid [Figure 17.6b (bottom)]. Qualitatively, one may say that here a small contact angle forms because the liquid rests on a surface that is of its own kind. Note that this is formally the same as that of Figure 17.6b (top) with media 2 and 3 interchanged. Such cases occur quite often; for example, many different vapors, including water and hydrocarbons, adsorb as a monolayer on mica, and these liquids have a small but finite contact angle on mica of $\theta_0 < 6°$.

If the interaction between 1 and 2 across 3 is montonically repulsive, the liquid droplet is now repelled from the surface [Figure 17.6c (top)], and we must put $W_{132} = 0$. Such situations lead to the complete spreading of a liquid on a surface and the development of thick wetting films [Figure 17.6c (bottom)], previously discussed in Sections 13.9 and 14.8 as they arise due to van der Waals and electrostatic forces, respectively.

Contact angles can often be changed by chemically modifying surfaces or by addition of certain solute molecules into the medium that adsorb on the surfaces (Chapter 19). For example, addition of "surface-active" molecules such as detergents to water can cause the contact angle to increase from 0 to 180° (see Figure 1.3d). When quartz is preheated above 300°C its hydrophilic surface silanol groups -Si(OH)-Si(OH)- give off water, leaving behind hydrophobic siloxane groups, -Si-O-Si-, and the contact angle rises from 0 to about 60°.

Electro-wetting. We have previously seen that spontaneous charge exchange, also known as contact electrification, can occur between two dissimilar surfaces, producing a capacitor (Figure 3.2) and an attractive force between the two surfaces (cf. Fig. 18.21). Similar effects occur when an external voltage or potential ψ is applied between two

surfaces or even across a single solid-liquid interface. The enhanced attraction is equivalent to an enhanced adhesion energy, which can be calculated from the general equation for the energy of an electric field, Eq. (3.12):

$$\text{Total electrostatic field energy} = \frac{1}{2}\varepsilon_0\varepsilon\int E^2 \mathrm{d}V, \tag{17.25}$$

where V is the volume of space where the field intensity is E. For a parallel-plate capacitor of area A and thickness δ, $V = A\delta$, and the field $E = \psi/\delta$ is uniform. We can therefore write for the electrostatic adhesion energy contribution per unit area:

$$W_{\text{el}} = \frac{1}{2}\varepsilon_0\varepsilon\psi^2/\delta \quad \text{C V m}^{-2}(\text{or J m}^{-2}). \tag{17.26}$$

For example, using the numerical values following Eq. (14.14) to model the Stern layer of Figure 14.4: $\delta = 0.2$ nm, $\varepsilon = 40$, $\sigma = 0.2$ C m^{-2}, we obtain $\psi = \sigma\delta/\varepsilon_0\varepsilon = 130$ mV and $W_{\text{el}} = 15.0$ mJ m^{-2}. Much higher values can be obtained when ψ is applied externally: 0.5 Volt would increase the above adhesion energy to ~220 mJ m^{-2}. When W_{el} is added to W_{12} in the Young-Dupré equation, Eq. (17.23), we can see that this will lead to a large decrease in the contact angle and/or total wetting of the surfaces by the liquid. Such *electro-wetting* and *electro-capillarity* effects are commonly used to control the contact angles and thus the wetting/spreading of liquids on surfaces (Mugele and Baret, 2005). However, the liquids and substrates need to be conducting (for example, electrolyte solutions on a metal substrate) in order for most of the field to fall across the gap between them.

17.5 Wetting of Rough, Textured, and Chemically Heterogeneous Surfaces

All the surfaces considered so far have been implicitly assumed to be both physically and chemically homogeneous. Most real surfaces are neither and, as we shall see, can also alter their shape and chemical composition during interactions—for example, when they come into or out of contact with another surface or liquid. To understand the subtle effects of chemical heterogeneity and surface roughness or "texture," we may initially consider the two simple situations depicted in Figure 17.8, the first a molecularly smooth but chemically heterogeneous surface, the second a textured but chemically homogeneous surface.

Effect of chemical heterogeneity on contact angles. Figure 17.8a shows a smooth surface that is chemically different on either side of the line at P. This difference manifests itself in different contact angles, θ_1 and θ_2, for a particular liquid L on these surfaces. The question is, What is the contact angle θ at P? The answer is that it is not uniquely defined, and can be anything between θ_1 and θ_2—that is, $\theta_1 \le \theta \le \theta_2$. To see how this arises, consider the line at P to have a small but finite width, as shown in the expanded part of Figure 17.8a, where the chemical composition of the surface varies continuously from pure 1 to pure 2. Let f_1 and f_2 (where $f_1 + f_2 = 1$) be the local fractions (surface densities) of components 1 and 2 inside the transition regime or strip. Writing

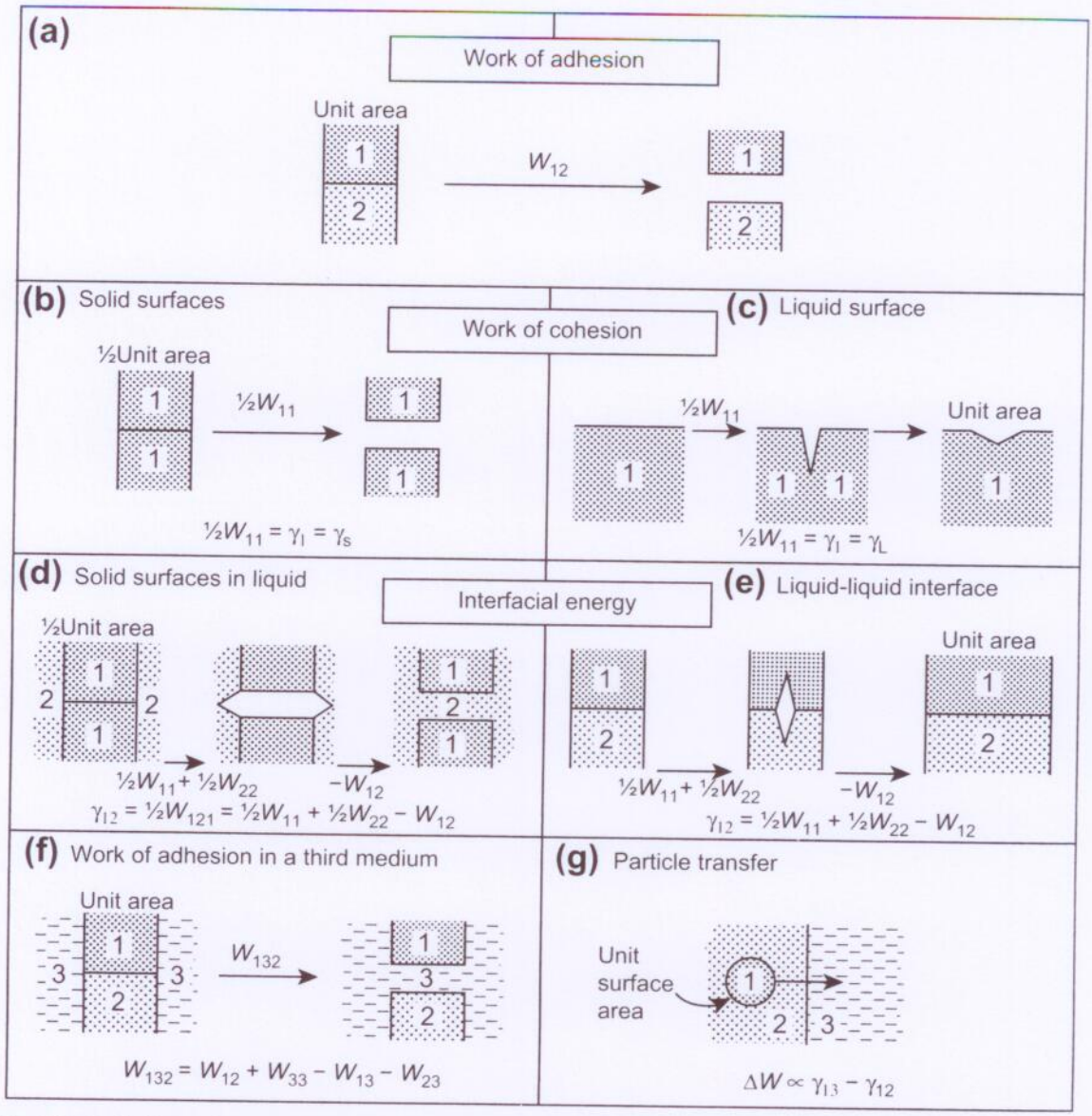

FIGURE 17.1 Definition of various energy terms associated with the adhesion of solid surfaces and the surface area changes of liquids. Note that W and γ are idealized thermodynamic quantities, assuming reversibility and smooth surfaces. In practice, only with liquids can the area be changed gradually and reversibly, as in (c). For solids, their adhesion, cohesion, and debonding processes, as in (a) or (b), usually involve plastic deformations with the dissipation of irreversible energy as heat. Note the positive sign of W (i.e., $W > 0$) for the work of adhesion/cohesion where, by convention, the reference state (of zero energy) is the contact state ($D = 0$), compared to the negative values for $W(D)$ and $w(r)$ where, again by convention, the reference states are at $D = \infty$, $r = \infty$.

where the spontaneous transfer of charge from one surface to another, dissimilar, surface generates an electrostatic attraction between the now oppositely charged surfaces (Dwight, 1997), a phenomenon that is also known as the "harpooning effect."

It is important to appreciate that when the process of increasing the surface area of a medium takes place in a foreign vapor, such as laboratory air, some adsorption of vapor

molecules (e.g., water, hydrocarbons) may take place on the newly created surface. This has the effect of lowering γ_S and γ_L from their values in a vacuum, and the surface energies in vapor are denoted by γ_{SV} and γ_{LV}. For example, when mica is cleaved in high a vacuum the surface energy is $\gamma_S \approx 4500$ mJ m^{-2}, but when cleaved in humid laboratory air it falls to $\gamma_{SV} \approx 300$ mJ m^{-2} (Bailey et al., 1970). The effects of adsorbed films and monolayers on surface energies are discussed in Chapter 19.

Interfacial energy. When two immiscible liquids 1 and 2 are in contact, the free energy change in expanding their "interfacial" area by unit area is known as their interfacial energy or interfacial tension γ_{12} or, in general, as γ_i. The energetics associated with this expansion process may be understood by splitting it into two hypothetical steps (Figure 17.1e): First, unit areas of media 1 and 2 are created, and are then brought into contact. The total free energy change γ_{12} is therefore

$$\gamma_{12} = \frac{1}{2}W_{11} + \frac{1}{2}W_{22} - W_{12} = \gamma_1 + \gamma_2 - W_{12}, \tag{17.2}$$

which is often referred to as the Dupré equation. As shown in Figure 17.1d, this energy is formally the same as that expended on separating two media 1 in medium 2 (W_{121}) or, conversely, of separating two media 2 in medium 1 (W_{212}). We may therefore also write

$$\gamma_{12} = \frac{1}{2}W_{121} = \frac{1}{2}W_{212}. \tag{17.3}$$

For a solid-liquid interface, γ_{12} is commonly denoted by γ_{SL}, so that the Dupré equation may be written as

$$\gamma_{SL} = \gamma_S + \gamma_L - W_{SL}. \tag{17.4}$$

Table 17.1 gives the surface and interfacial energies of some common substances. These values are always positive. When γ or γ_{12} is negative, the area wants to expand indefinitely, which means that 1 and 2 are miscible—that is, the interface eventually disappears (evaporates or dissolves).

If only dispersion forces are responsible for the interaction between media 1 and 2, we have previously seen that to a good approximation

$$W_{12} \approx \sqrt{W_{11}^d W_{12}^d} \approx 2\sqrt{\gamma_1^d \gamma_2^d} \tag{17.5}$$

so that Eq. (17.2) now becomes

$$\gamma_{12} \approx \gamma_1 + \gamma_2 - 2\sqrt{\gamma_1^d \gamma_2^d}, \tag{17.6}$$

where γ_1^d and γ_2^d are the dispersion force contributions to the surface tensions. Fowkes (1964) and Good and Elbing (1970) estimated that for water, the dispersion contribution to the total surface tension is 20 ± 2 mN m^{-1} or about 27% of the total. Note the near agreement between this value and the probably fortuitous theoretical estimates of 24 and 25% obtained in Tables 6.3 and 13.4. The remaining 53 mN m^{-1} arises from nondispersion (i.e., polar and H-bonding) interactions. Since water and hydrocarbon

Table 17.1 Surface and Interfacial Energies Selected from Different Classes of Materials at 20–25°C (mJ m^{-2})[a]

Liquid 1	Surface Energy γ_1	Interfacial Energy γ_{12}
		With water, H_2O ($\gamma_2 = 72$–73)
n-hexane to *n*-hexadecane (sat) C_nH_{2n+2}	18–27	50–53
1-hexene to *1*-dodecene (unsat) C_nH_{2n}[b]	18–25	44–48
iso-alkanes/paraffins (branched) C_nH_{2n+2}[b]	18–22	~48
Cyclohexane C_6H_{12} 20°C	25	51
Paraffin wax (solid) $C_{20}H_{42}$ to $C_{40}H_{82}$[c]	25	~50
PTFE (solid) $CF_3(CF_2)_nCF_3$ 20°C c	19	50
Carbon tetrachloride CCl_4 20°C	27	45
Benzene C_6H_6, toluene $C_6H_5CH_3$	28	34–36
Chloroform $CHCl_3$ 20°C	27	28
Diethyl ether $C_2H_5OC_2H_5$ 20°C	17	11
Cyclohexanol $C_6H_{11}OH$ 20°C	32	4
Mercury Hg 20°C	486	415
		With tetradecane, $C_{14}H_{32}$ ($\gamma_2 = 26$)
Water, H_2O	72–73	53
Glycerol (1,2,3 propane-triol) $C_3H_5(OH)_3$[d]	64	31–36
1,3 propane-diol $HO(CH_2)_3OH$	49	21
Ethylene glycol (1,2 ethane-diol) $C_2H_4(OH)_2$	48	18–20
1,2 propane-diol $CH_3CH(OH)CH_2OH$	38	13
Formamide $H(CO)NH_2$	58	29–32
Methyl-formamide $H(CO)NH(CH_3)$	40	12
Dimethyl-formamide $H(CO)N(CH_3)_2$	37	5

[a]Values compiled from standard references, especially TRC Thermodynamic Tables for Hydrocarbons (1990), Jańczuk et al., (1993), Landolt-Börnstein (1982), Zografi and Yalkowsky (1974).
[b]Note that C = C double bonds (unsaturation) and branching have only a small effect on the surface and interfacial energies of hydrocarbons with water.
[c]Note that surface and interfacial tensions need not change when one or both of the phases change from liquid to solid.
[d]Also glycol, glycerine.

attract each other mainly via dispersion forces, the interfacial tension of a hydrocarbon-water interface should therefore be given by Eq. (17.6). Thus, for octane-water, putting $\gamma_1^d = 21.8$ mN m^{-1} and $\gamma_2^d = 20$ mN m^{-1}, we calculate

$$\gamma_{12} \approx 21.8 + 72.75 - 2\sqrt{21.8 \times 20} \approx 52.8 \text{ mN m}^{-1}$$

which is very close to the measured value of 50.8 mN m^{-1}. This good agreement is obtained for many hydrocarbon-water interfaces, but the agreement is not so good for unsaturated hydrocarbons and aromatic molecules such as benzene and toluene (Fowkes, 1964; Good and Elbing, 1970).

Work of adhesion in a third medium, the "spreading pressure." It is left as an exercise for the reader to establish that the energy change on separating two dissimilar media 1 and 2 in medium 3 (Figure 17.1f) is given by

$$W_{132} = W_{12} + W_{33} - W_{13} - W_{23} = \gamma_{13} + \gamma_{23} - \gamma_{12}. \tag{17.7}$$

Note that W_{132} can be positive (attraction between 1 and 2 in 3) or negative (repulsion between 1 and 2 in 3).

A negative W_{132} is often referred to as a "spreading pressure" or "spreading coefficient," commonly denoted by S, C, or π, because when W_{132} is negative ($S > 0$), liquid 3 will displace liquid 2 and "spread on" or "totally wet" the surface of 1. This also implies that $\gamma_{13} + \gamma_{23} < \gamma_{12}$, which means that the two interface of 1|3 and 2|3 have a lower energy than the single interface of 1|2 or, alternatively, that the 1|2 interface will spontaneously split into two interfaces by the penetration of medium 3.

However, when W_{132} is positive ($S < 0$), we have $\gamma_{13} + \gamma_{23} > \gamma_{12}$, which is a necessary but not a sufficient or strong enough condition to allow us to conclude that medium 2 will spread on medium 1: partial spreading, with a contact angle between 0 and 180° (see Figure 17.6) is also a possibility, where both media 2 and 3 are in contact with 1. For full spreading of medium 2 on medium 1 we require that $\gamma_{13} > \gamma_{12} + \gamma_{23}$—that is, $W_{123} < 0$.

Note that if medium 3 is a vacuum, $W_{132} \rightarrow W_{12}$, $\gamma_{13} \rightarrow \gamma_1$, $\gamma_{23} \rightarrow \gamma_2$, Eq. (17.7) reduces to Eq. (17.2) as expected, where W_{12} is always positive.

Surface energy of transfer. When a macroscopic particle 1 moves from medium 2 into medium 3 (Figure 17.1g) the change in energy per unit area of the particle's surface is

$$\Delta W = \left(W_{12} - \frac{1}{2}W_{22}\right) - \left(W_{13} - \frac{1}{2}W_{33}\right) = \gamma_{13} - \gamma_{12}, \tag{17.8}$$

where $(W_{12} - \frac{1}{2}W_{22})$ is the energy required to first separate unit areas of media 1 and 2 and then bring into contact the newly created free surfaces of medium 2, and where $-(W_{13} - \frac{1}{2}W_{33})$ is the reverse operation for medium 1 with medium 3.

17.2 Adhesion Energies versus Adhesion Forces

We have already noted the conceptual differences between energies and forces. These differences are particularly manifest in adhesion and wetting phenomena, as illustrated in Worked Example 17.1.

Worked Example 17.1

Question: Consider the two adhering polymer surfaces of Figure 17.2 where the initial and final (fully separated) states are the same but where the paths between them are different. What are the adhesion forces in each case? Assume a Hamaker constant of $A = 6.5 \times 10^{-20}$ J and a square area of 1 cm × 1 cm.

Answer: Path (a) involves planar separation where the van der Waals adhesion force is given by $F_{ad} = A \times \text{area}/6\pi D_0^3 = (6.5 \times 10^{-20}) \times (0.01)^2/6\pi(1.65 \times 10^{-10})^3 = 7.7 \times 10^4$ N. Concerning the net change in energy, this is the same in both cases and is given by $W_{ad} = A \times \text{area}/12\pi D_0^2 = 6.3 \times 10^{-6}$ J. However, path (b) involves peeling of the surfaces over a distance of

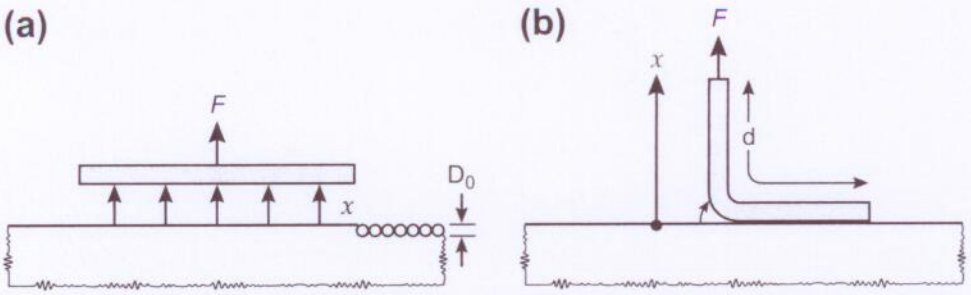

FIGURE 17.2 Two different paths for surfaces to separate, involving the same net change in energy ΔW or W_{ad} but requiring very different "adhesion" forces, F. In general, since $\Delta W = \int F dx$, we can see that depending on the path taken, which is prescribed by x, the force can be large or small as well as continually changing during the separation. Furthermore, even for a given path, the force can depend on the time or rate of separation, and can be higher or lower than the values calculated in Worked Example 17.1. This example illustrates how a soft adhesive polymer film[1] on a hard ceramic plate can provide a very strong adhesion force even when the surface energy of the polymer is low (i.e., involving only weak van der Waals forces).

$d = 1\text{ cm} = 0.01\text{ m}$ at a constant force of $F = W_{ad}/d = 6.3 \times 10^{-4}\text{ N}$ (cf. nonspecific bridging forces in Figures 16.8 and 16.9), which is 8 orders of magnitude less than for the planar separation.

■ ■ ■

Worked Example 17.1 shows how the same starting and ending states, and energy change, can nevertheless involve very different forces depending on the paths taken. This particular example also has practical implications: adhesive tape can be peeled away with little force as in Figure 17.2b, while an adhesive ceramic tile requires a substantially greater force even though the adhesive polymer layer may be the same. In the latter case, the stiff tile causes the surfaces to separate all at once, effectively mimicking the path of Figure 17.2a. Clearly, when referring to the "strength" of an interface or bond, one must specify whether one is talking about the energy or the force needed to break the contact.

An oft-asked question is: Since surfaces in a liquid separate in a vacuum before any liquid molecules can get between them (cf. Figure 15.4), shouldn't the adhesion force and energy be given by the interaction in a vacuum? Strictly, yes: if the two surfaces were truly flat and rigid and separated while remaining parallel to each other, as in Figure 17.2a, the initial force *would* be that in a vacuum, falling as soon as the first layer of molecules enters the gap, then oscillating to zero as $D \to \infty$. But in practice two surfaces almost always separate by peeling, where the solvent molecules immediately enter between the surfaces at the bifurcation line. Similar effects occur in vapor due to adsorption; for example, the measured adhesion force of peeling or cleaving a mica sheet in air is less than 10% of the value in a vacuum.

The path taken is not only geometry-dependent but also rate-dependent: for very fast separations the adhesion force can reach very high values if there is not enough time for

[1]A Pressure Sensitive Adhesive (PSA) is supposed to stick without any external pressure.

the surfaces to deform so that they can peel away, or for the solvent or vapor molecules to enter the gap or bifurcation line during the peeling process. Such large and rapidly changing adhesion forces can give rise to the phenomenon of cavitation in liquids (which can result in irreversible surface damage). Nonequilibrium and rate-dependent interactions lead to hysteresis effects, where again very different paths and forces can be experienced depending on the rates at which surfaces are moved, either normally (toward or away) or laterally relative to each other (friction forces). These issues are discussed in various other sections and chapters as they arise in different systems (see the Index). The important point to note is that in each of the detachment processes discussed above the net energy change is the same but the forces very different.

The thermodynamic "surface energy" and/or "surface tension" of a liquid is defined by a single parameter γ that can be expressed in units of energy (J m^{-2}) or, dimensionally equivalently, in units of force (N m^{-1}). This is somewhat unfortunate because it can lead to confusion, especially when considering rate-dependent nonequilibrium processes (Sections 17.6 and 17.8), nonplanar surfaces (Section 17.9), and surfaces with monolayers on them (Chapters 19 and 20). Here we shall consider some of the different ways of looking at the molecular origins of surface energy and tension, which will provide the basis for the discussions of the above three phenomena. Figure 17.3 shows three different ways of looking at how the concept of surface energy and tension γ arise at a bulk liquid-vapor interface. The three scenarios are equivalent but only when the following three conditions are satisfied: planar surfaces, pure single-component liquids, and equilibrium conditions.

In the first scenario, Figure 17.3a, two unit areas are brought together involving a change in energy of ΔW while eliminating *two* unit areas. In this case we can define $\gamma = \frac{1}{2}\Delta W$ per unit area, which is in units of J m^{-2}.

In the second scenario, Figure 17.3b, we consider a single surface with two imaginary parallel lines of length z going into the paper that attract each other with a force F per unit

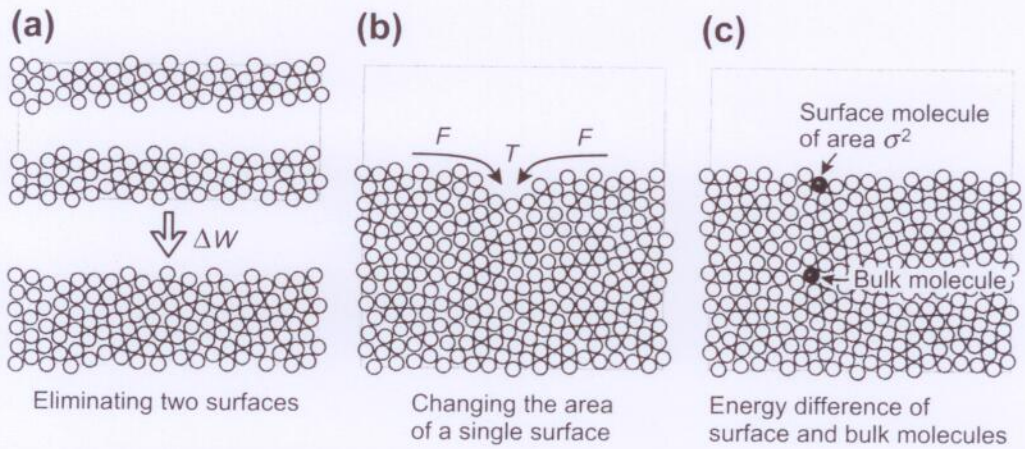

FIGURE 17.3 Different ways of looking at the origin of surface energies and surface tension forces of pure (single-component) systems. The situation can be very different when a liquid surface contains a monolayer or sub-monolayer of adsorbed molecules that are "insoluble" in the bulk liquid (see insoluble monolayers in Chapter 19).

length or tension, T. On closing the gap between the two lines by a lateral distance x, the area of the surface has decreased by $A = zx$ and the energy by $F \times$ length of line $\times$ distance moved $= Fzx = FA$. Assuming that we can equate this energy with the energy γA of the first scenario, we find that F is the same as the γ but now in units of force per unit length ($\mathrm{N\,m^{-1}}$). This is the way surface tension was first conceived.

The third scenario also involves a single surface, Figure 17.3c, but with no motion or change in area, just a consideration of the equilibrium difference in the energy between a molecule at the surface and one in the bulk. In the bulk, let each molecule share 12 bonds of energy w with its nearest neighbors. On the surface the number of shared bonds will be 9. The difference is 3 shared bonds per molecule, or $1\frac{1}{2}$ full bonds per molecule. Thus, the energy per unit area relative to the bulk reference state is $\gamma = 3w/2\times$ area per molecule which is the same as Eq. (13.40). We therefore see that the three scenarios of Figure 17.3 lead to the same numerical values for γ, but only under the conditions mentioned above.

The surface energies, tension, and stresses of surfaces with adsorbed species on them (e.g., surfactant and lipid monolayers on water) are described in Chapters 19 and 20. The surfaces of such two-component systems often exhibit very different properties from the single-component systems discussed here; for example, the monolayers may be elastic, with a tension that changes with the surface area rather than being independent of it.

17.3 Highly Curved Surfaces and Interfaces: Clusters, Cavities, and Nanoparticles

Here we shall investigate the validity of applying the concept of surface energy and tension to highly curved surfaces such as clusters, droplets, nanoparticles, cavities (holes, voids, bubbles) and even isolated molecules. Clearly the idea of a surface tension as exemplified in Figure 17.3c cannot be applied to a single atom or molecule since there is no "bulk energy" to compare the surface energy with. An atom or molecule surrounded by 12 nearest neighbors is the smallest cluster where such a comparison can be made.

But the concept of a surface or interfacial energy can be applied already to single molecules, since there is always an energy change associated with transferring a molecule from one medium to another or one location to another (as in Figure 17.1g), and this process can always be expressed in terms of $4\pi a^2\gamma$ or $4\pi a^2(\gamma_{13} - \gamma_{12})$, where a is the molecular radius. For small droplets or clusters two immediate questions arise: (1) How close will the surface energy of a cluster be to that of the planar bulk interface, and (2) how should one define a cluster—in terms of the number of molecules or the radius? If, as is commonly done, by the radius, problems of where to define the surface at the atomic or molecular level arise when, for example, we also want to define the radius of a hole vacated by a cluster or of one liquid in another since the atoms intercalate at the interface (see below).

Let us start by considering the reference planar surface: if $-w$ is the pair energy at molecular contact, then for a planar close-packed surface lattice, with three unsaturated bonds per surface molecule, the surface energy was previously found to be given by Eq. (13.40) as

$$\gamma \approx \sqrt{3}w/\sigma^2 = \sqrt{3}w/4a^2 \approx 0.43w/a^2 \text{ J m}^{-2} \qquad \text{for a planar surface,} \tag{17.9}$$

where $\sigma = 2a$ is the molecular diameter. In contrast, for a single, isolated molecule, with 12 unsaturated bonds, its effective surface energy is

$$\gamma \approx 12w/2(4\pi a^2) \approx 0.48w/a^2 \text{ J m}^{-2} \qquad \text{for a single atom,} \tag{17.10}$$

while for a cluster of 13 molecules, with seven unsaturated bonds per each of the 12 surface molecules (Figure 17.4), we obtain

$$\gamma \approx 7 \times 12w/2[4\pi(3a)^2] \approx 0.37w/a^2 \text{ J m}^{-2} \qquad \text{for a 13-atom cluster,} \tag{17.11}$$

which is only slightly smaller than the value for the planar surface. Thus, we arrive at the remarkable conclusion that the magnitude of the effective surface energy γ of a very small cluster, or even an isolated molecule, is within 15% of that of the planar macroscopic surface. We encounter various experimental manifestations of this phenomenon in Section 8.5 and elsewhere in this book.

Equation 17.11 is qualitatively consistent with the Tolman Equation which gives the surface energy of a spherical droplet of radius R as (Tolman, 1949; Rowlinson and Widom, 1989).

$$\gamma(R) \approx \gamma(\infty)/(1 + \delta/R) \approx \gamma(\infty)(1 - \delta/R), \tag{17.12}$$

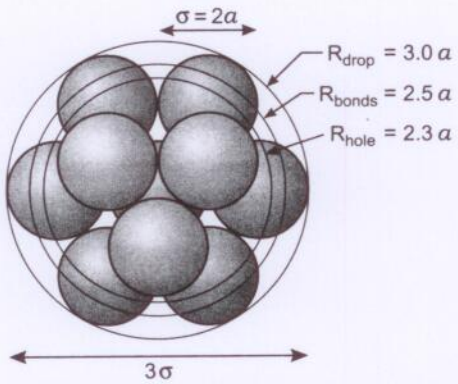

FIGURE 17.4 Cluster of 13 atoms or molecules: one central atom surrounded by 12 close-packed neighbors, six in the plane of the page with three above and three below. Note that each of the 12 surface atoms has 5 contact points with its neighbors in the cluster and therefore 7 with the next layer (of 42 molecules, not shown). These 84 contact points with the third layer may be thought of as the centers of the interatomic bonds. The number of spheres in complete-shell icosahedra are: 1, 13, 55, 147, 309, 561, . . . , and 74% of the volume is occupied. In 2D the sequence is: 1, 7, 19, . . . , and 91% of the area is occupied. In practice, real clusters are rarely close-packed structures.

where $\gamma(\infty)$ is the surface energy of the planar surface ($R = \infty$), and δ is an atomic-scale dimension. For the 13-atom cluster of radius $R = 3a$ our analysis would give $\gamma(R)/\gamma(\infty) = 0.37/0.43 = (1 - \delta/3a) \Rightarrow \delta = 0.4a$. The Tolman equation remains controversial: it is difficult to test experimentally, and its extension to cavities or to droplets in another medium, where γ_i replaces γ, is not obvious.

The cluster of Figure 17.4 shows a central atom surrounded by six atoms in the same plane, with three above and three below. This type of packing is referred to as hexagonal close packed (HCP), where, if continued, the "bilayers" alternate indefinitely. However, one can see that the three atoms in the lower plane, which are not seen because they are shielded by the three in the upper plane, could be rotated by 60° yet still give a close-packed structure. This type of packing is referred to as face centered cubic (FCC) where, if continued, "trilayers" alternate indefinitely. When next-nearest neighbor energies are considered one immediately sees that the HCP cluster is energetically favored over the FCC because the atoms of the two outermost layers are closer together. One would therefore expect spherical atoms, molecules, and nanoparticles to pack into HCP lattices rather than FCC, but both occur naturally, sometimes with a transition between them at some particular temperature. The reasons for these effects are subtle—the energy differences are typically $\sim 10^{-3}\, kT$ per particle—and have been attributed to 3- and higher-body interactions, multipole interactions, and entropy effects (Niebel and Venables, 1974; Woodcock, 1997).

The above discussion becomes even more complex when extended to curved surfaces that are not isolated droplets, such as the asperities on a rough surface, and to concave surfaces such as cavities or holes. Figure 17.5 shows a spherical cluster or droplet and its complementary hole. While the total surface energies of a droplet and its complementary cavity may be the same, convex and concave surfaces nevertheless exhibit both

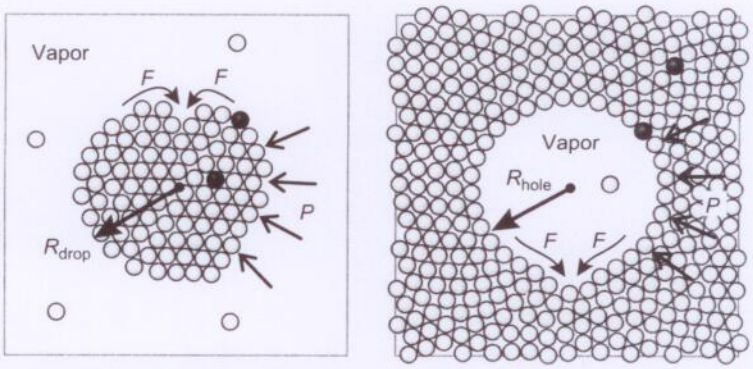

(a) Complementary droplet of hole (b) (b) Complementary hole of droplet (a)

FIGURE 17.5 Small spherical cluster or nano-droplet (left) and complementary cavity or hole (right). For additive nearest-neighbor pair potentials, the total surface energy of the cluster and its complementary cavity (the one it was extracted from) must be the same, but other surface properties can be very different. For example, the surface energy *per surface atom* is greater in droplets or convex surfaces than in holes or concave surfaces because the former has fewer bonds than the latter. In contrast, the surface energy *per unit area* is somewhat arbitrary, since it depends on where the convex and concave radii are defined.

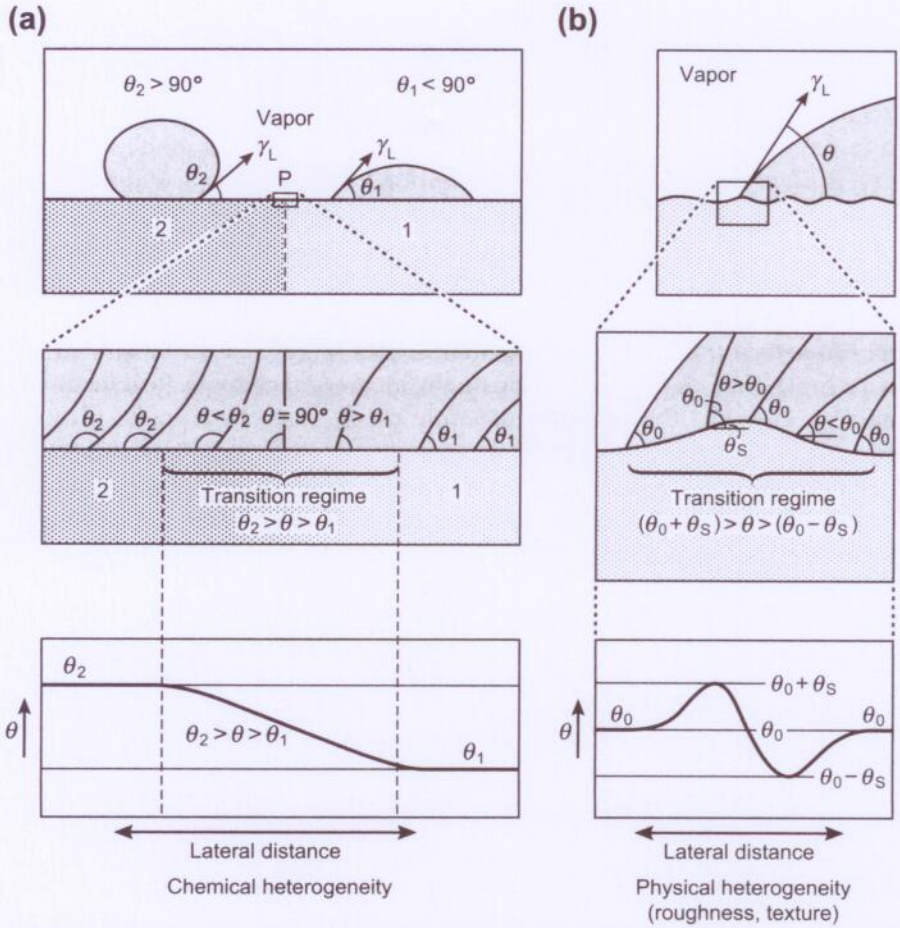

FIGURE 17.8 **(a)** Effects on the contact angle at a line separating two chemically different regions of a smooth surface. **(b)** Effect on the contact angle at a ridge separating two chemically homogeneous regions of an otherwise smooth surface. Note that the contact angle will be different depending on whether the liquid droplet is approaching from the left or right and also whether it is advancing or receding. The chemical and topographical heterogeneities shown here have been oversimplified to occur at a 1D line; real surfaces are usually much more complex, exhibiting heterogeneities in both 2D and 3D.

$\gamma_L(1 + \cos\theta_1) = W_{1L} \approx \sqrt{W_1 W_L}$ and $\gamma_L(1 + \cos\theta_2) = W_{2L} \approx \sqrt{W_2 W_L}$ for the Young-Dupré equations for the pure surfaces, then within the strip:

$$\gamma_L(1 + \cos\theta) \approx \sqrt{(f_1 W_1 + f_2 W_2) W_L} = \sqrt{f_1 W_1 W_L + f_2 W_2 W_L}, \tag{17.27}$$

which gives the following general relation for the contact angle at a chemically heterogeneous surface:

$$(1 + \cos\theta)^2 = f_1(1 + \cos\theta_1)^2 + f_2(1 + \cos\theta_2)^2. \tag{17.28}$$

This equation is similar to the Cassie Equation:

$$\cos\theta = f_1\cos\theta_1 + f_2\cos\theta_2 \tag{17.29}$$

which is more appropriate for surfaces with chemically distinct—that is, microscopic rather than nanoscopic, patches of compounds 1 and 2 (Cassie, 1948; Israelachvili and Gee, 1989). Both equations give the same limiting values as $f_1 \to 1$ and $f_2 \to 1$.

Returning to Figure 17.8a, we can see that within the strip at P the contact angle can take on any value between θ_1 and θ_2, an effect that is one of the main causes of contact line "pinning" and contact angle hysteresis and hysteresis effects in adhesion and capillary forces (see Sections 17.6 and 17.8 and Problem 17.2).

Effects of surface topography on contact angles. Figure 17.8b illustrates the similar effects of a simple line ridge or depression on the local contact angle. Real textured surfaces are usually more ornate: they can be randomly rough, have a particular texture, or have a periodic profile or "pattern" such as the one shown in Figure 17.9. Each of these topographies, even the simplest periodic one, can result in complex and varied effects, including different apparent contact angles θ and wetting properties, hysteresis, sudden instabilities, time-dependent effects, and different local deformations of the surfaces (see later).

For textured surfaces the molecular or "real" area of liquid-solid contact is usually no longer the same as the macroscopic or "projected" area, defined by the circle where the macroscopic contact angle θ is defined—a distinction that does not arise with smooth surfaces. For such surfaces, we may replace W_{132} by ϕW_{132} in Eq. (17.17), where ϕ is the fraction by which the real area is greater or less than the projected area. For a liquid droplet on a surface in vapor the Young-Dupré equation then becomes

$$\gamma_L(1 + \cos\theta) = \phi W_{SL} \tag{17.30a}$$

which leads to

$$(1 + \cos\theta) = \phi(1 + \cos\theta_0), \tag{17.30b}$$

where W_{SL} and θ_0 are the values for molecularly smooth surfaces. Equation (17.30b) may be compared with the Wenzel Equation (Wenzel, 1936): $\cos\theta = \phi\cos\theta_0$ which, however, appears to be unphysical in that it predicts no effect of roughness when $\theta_0 = 90°$.

The problem of roughness usually reduces to one of determining the value of the dimensionless parameter ϕ for a textured surface, where ϕ can be less or greater than 1. According to Eq. (17.30) for $\phi > 1$ the macroscopic contact angle θ is lower than θ_0, while for $\phi < 1$ it is higher (for the simple reason that the liquid-surface adhesion per unit projected area must be higher or lower, respectively).

In spite of the generality and simplicity of Eq. (17.30) for macroscopic droplets the general situation is complex because ϕ is usually difficult to predict. Figure 17.9 shows a surface with a microscopically wavy but chemically homogeneous surface—that is, where the local (real) contact angle θ_0 is less than 90° in region (a) and greater than 90° in region (b). For each case we can envisage three scenarios: (1) a macroscopic droplet of liquid is placed on the surface, (2) a nanoscopic droplet is placed on the surface, and (3) the

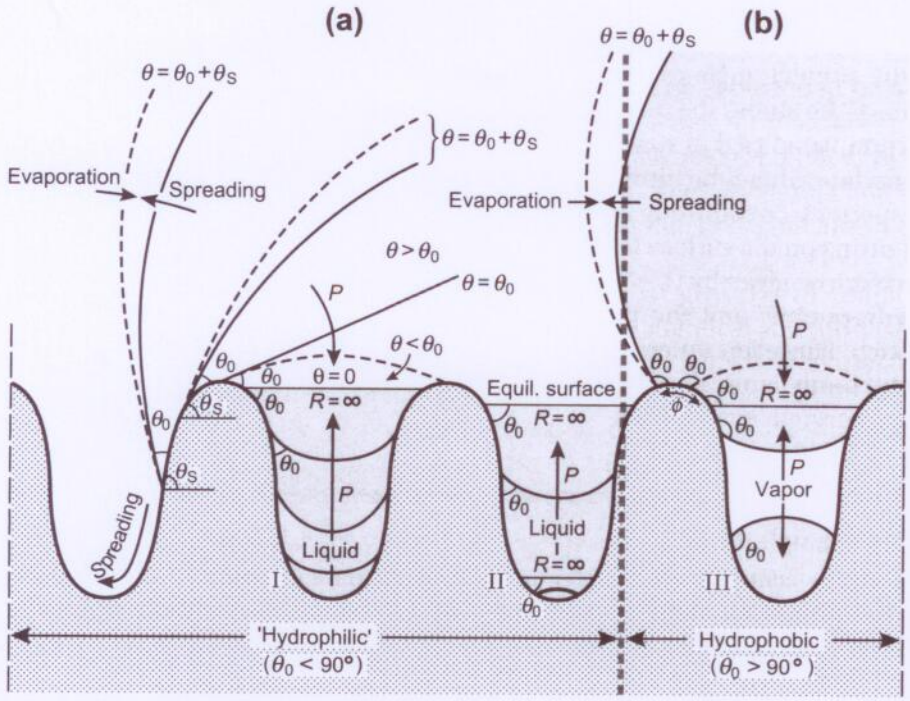

FIGURE 17.9 Wetting and spreading of a liquid on a periodically patterned surface when (i) a large droplet is placed on the surface, and (ii) the liquid condenses from saturated vapor where the ultimate, thermodynamically equilibrium, meniscus is flat—that is, $R = \infty$ (see Kelvin radius). **(a)** When the liquid has a low intrinsic contact angle, θ_0, it will immediately spread and fill all the holes or wells. After the initial spreading, the concave liquid surfaces will grow (by condensation), while any convex surfaces will slowly evaporate, each driven by the Laplace pressures P in the directions shown. The final state will be a liquid surface with zero apparent contact angle ($\theta = 0$) and zero Laplace pressure ($R = \infty$). **(b)** When the liquid has a high intrinsic contact angle, θ_0, all liquid surfaces are convex, as shown. The Laplace pressure drives all these surfaces to evaporate while reducing the real contact area to zero ($\phi \to 0$). Note that very high local Laplace pressures can cause elastic or plastic deformations of solid surfaces. The situations depicted here are more complex when the vapor is not saturated.

liquid condenses on the surface from vapor. For each of these scenarios we may further consider the initial (mechanical equilibrium) and final (thermodynamic equilibrium) configurations. Even ignoring the effects of gravity, the many different variables of this system (not to mention the crucial details of the surface topography) makes it difficult to arrive at any general conclusions regarding ϕ, and only a few of the more commonly encountered situations will be considered (see also Problems 17.8, 17.9, 17.12 and 17.28).

For liquids of low intrinsic contact angles, say $\theta_0 = 10°$, Eq. 17.30 gives $\cos\theta = 1.9848\phi - 1$. Thus, θ can be zero, small or large depending very delicately on the precise value of ϕ. For example, for $\phi = 1.000$, we obtain $\theta = 10°$, as expected. For $\phi < 1.000$ the contact angle θ will be greater than 10°, while for $\phi > 1.008$ the contact angle will be zero—that is, the liquid will completely wet the surface ($\theta = 0$). This is the situation that occurs in practice for low θ_0 systems on rough or textured surfaces (for example, water

on hydrophilic surfaces) once thermodynamic equilibrium has been attained, as illustrated in Figure 17.9a. Figure 17.9a also illustrates some nonequilibrium situations where the contact angle can be significantly higher than the intrinsic angle θ_0.

Figure 17.9b shows the quite different situation where θ_0 is greater than 90°, when the equilibrium value of ϕ is now smaller than 1. As an example, consider a rough hydrophobic surface where the intrinsic water contact angle is $\theta_0 = 90°$ and where only the tops of the asperities, constituting 20% of the projected area, are actually contacted by a water droplet sitting on the surface (see point ϕ in Figure 17.9b). The macroscopic contact angle will therefore be given by $(1 + \cos\theta) = \phi = 0.2 \Rightarrow \theta = 143°$. Such surfaces are referred to as superhydrophobic, and the phenomenon is also known as the Lotus Effect (see also Fig. 15.16g). However, unless the vapor is supersaturated, convex water droplets should not be thermodynamically stable on hydrophobic (or any) surfaces and should eventually disappear through evaporation.

Worked Example 17.5

Question: The contact angle of water on the planar surface of Figure 17.9 is 30°. The central cavity I is exposed to saturated water vapor. Sketch the path taken by the water meniscus or droplet in this cavity. Ignore gravitational effects and the possible involvement of other cavities.

Answer: The path taken by the meniscus as liquid water condenses from vapor is shown by the lines $a \rightarrow e$ in Figure 17.10, where $\theta = 30°$ in each case. State a is unstable and will tend to shrink (evaporate), b is metastable, c and d continue to grow, e is the stable state, and f is unstable and will shrink back to e. The path involves the nucleation of droplet b before further growth can proceed. The nucleation is energetically unfavorable and will be the rate-limiting part of the whole process—the greater the volume of water that needs to be nucleated, the longer will be this time.

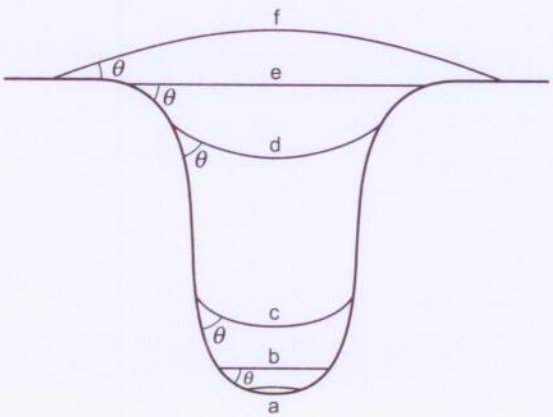

FIGURE 17.10

17.6 Contact Angle Hysteresis

The contact angle, being a thermodynamic quantity, should be expected to be a unique value for any particular system. But it is often found that when an interface advances along a surface, even a molecularly smooth surface, the "advancing" contact angle, θ_A, is larger than the "receding" angle, θ_R. This is known as *contact angle hysteresis*, and we have already seen in Figures 17.8 and 17.9 how it can come about due to chemical and physical heterogeneities of surfaces.

Figure 17.11 shows these and two additional effects that give rise to contact angle hysteresis: the additional effects being due to *changes* in the chemical and physical nature of the surfaces after they have come into contact with a liquid or another material (rather than having these properties fixed as in Figures 17.8 and 17.9). Other physico-chemical reactions, not shown in Figure 17.11, can also produce contact angle hysteresis—for example, when surfactant adsorbs to a surface from an advancing liquid. The role of time, advancing and receding rates, and previous history enter naturally into any contact angle hysteresis that is due to such effects since the changes are invariably associated with some characteristic relaxation, adaptation, or adsorption time.

Contact angle hysteresis can be very large, with advancing and receding angles sometimes differing by more than 90°, and it is often very difficult to tell which effect is responsible. When a receding interface is not retracing its original advancing or spreading path, the process is not thermodynamically reversible, and it is generally not immediately obvious which, if any, of the two contact angles represent the truly equilibrium value. The matter is not easy to resolve experimentally—for example, by allowing very long equilibration times—since advancing and receding angles can be stable for very long times. As the previous discussion and figures have shown, only on perfectly smooth and chemically homogeneous surfaces can we hope to obtain the "true" angle (and then only if the surfaces are infinitely rigid and chemically inert). There is also the nagging matter that a droplet with a convex surface cannot be at thermodynamic equilibrium with its vapor: it can only be in mechanical equilibrium.

The phenomenon of contact angle hysteresis is a manifestation of a much more general effect: the hysteresis in the adhesion energy W of two phases, where one or both of the phases are solid (Figure 17.11d). For a liquid droplet on a surface, it is the different values of W for the advancing and receding liquid with the surface that results in the different values for θ via the Young-Dupré equation, Eq. (17.23). For two solids, the difference manifests itself in different (irreversible) loading and unloading energies, time-dependent adhesion forces, and energy-dissipating friction forces (Chapter 18).

The existence of hysteresis and irreversibility usually means that a system is trapped in a transient or metastable nonequilibrium state. In the case of a liquid droplet on a solid surface this can be due to mechanical or chemical effects, as illustrated in Figure 17.12. Let us first consider the three liquid phases of Figure 17.12a. At the three-phase boundary, the three contact angles will be uniquely determined by the three interfacial tensions

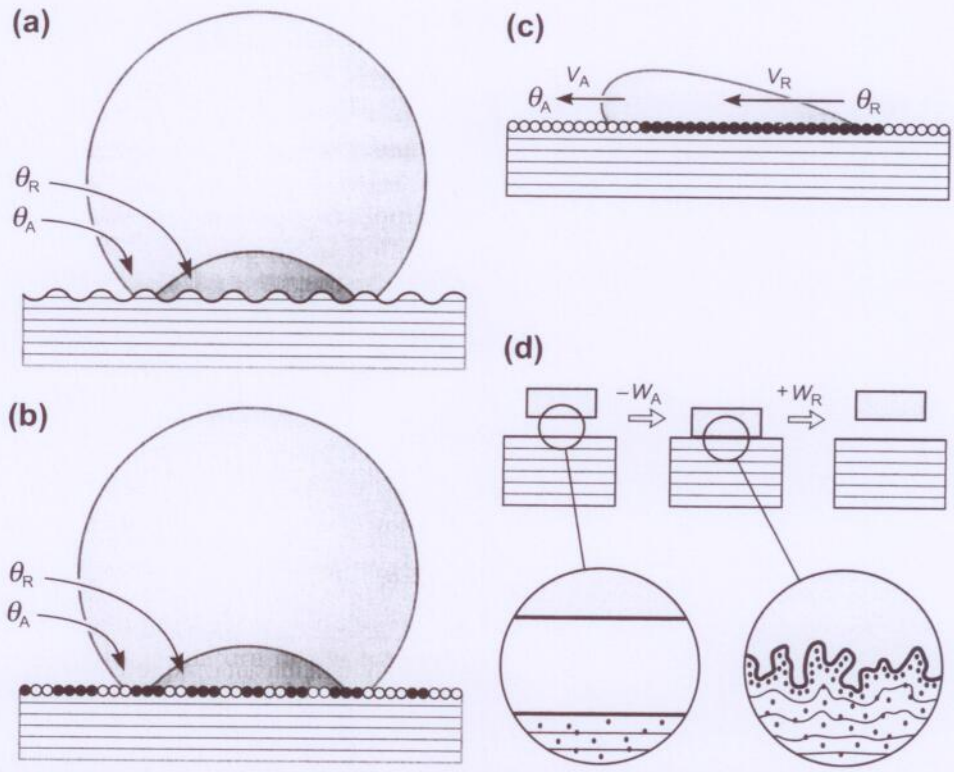

FIGURE 17.11 Contact angle and adhesion hysteresis. **(a)** Effect of surface roughness: liquid droplets on a rough surface where the microscopic contact angle is 90° in each case but the macroscopic (measured) advancing and receding contact angles, θ_A and θ_R, are very different. **(b)** Effect of chemical heterogeneity: droplets on a smooth but chemically heterogeneous surface where the adhesion energy W is different at different places. **(c)** The orientation of surface chemical groups often depends on the phase they are exposed to, resulting in molecular rearrangements and different adhesion energies and contact angles at the advancing and receding ends of the moving droplet. These angles are rate- and previous history–dependent—that is, depending both on the velocity of the moving "three-phase boundaries," V, and the time the liquid has been in contact with the surface. **(d)** Interdiffusion and interdigitation, especially of viscoelastic and polymer-like materials, resulting in different adhesion energies on approach W_A and separation (retraction) W_R, which is analogous to the advancing and receding energies in panel (c). Note how both surfaces may look "perfect" before and after they are in contact but totally different when *in* contact.

according the triangle of forces rule or, equivalently, the requirement of the uniformity of the Laplace pressure in Liquid 1. When this condition is satisfied, true thermodynamic equilibrium will have been attained. Now consider the situation where the lower surface is a solid and where the three interfacial energies are unchanged. Clearly, the *equilibrium* geometry should also be unchanged, but in practice, if the solid is rigid and undeformable, the geometry will depend on the shape of the solid surface. Actually, a real solid *will* deform elastically or plastically with time; for example, starting from Figure 17.12b the system will slowly deform and approach the true equilibrium geometry of Figure 17.12c, but this may take billions of years.

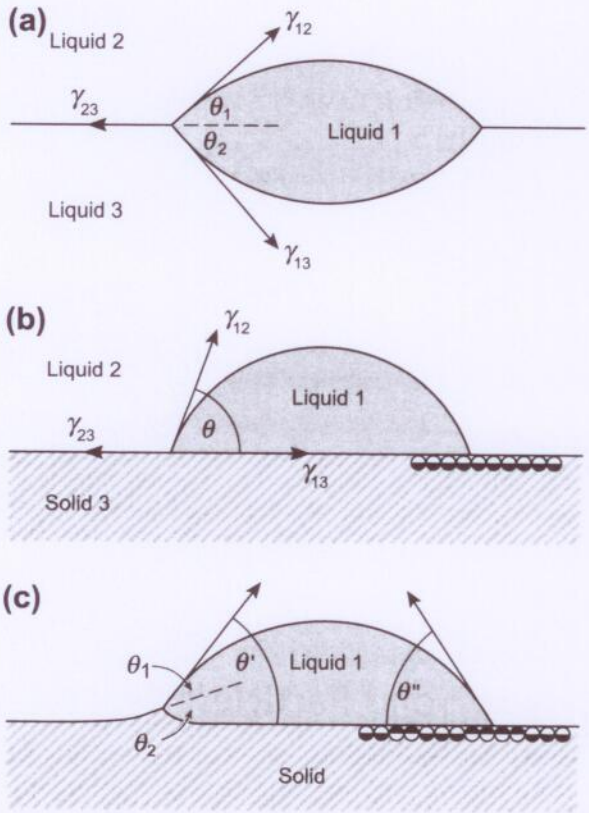

FIGURE 17.12 **(a)** Equilibrium configuration of liquid droplet (or lens) on another liquid. **(b)** Nonequilibrium (but mechanically stable) configuration of liquid droplet on a solid surface. Equation 17.31 shows that θ will be greater than θ_1 but less than $(\theta_1 + \theta_2)$. **(c)** Microscopic and molecular-scale deformations that can occur, usually at the three-phase boundary, to relax the vertical component of the interfacial tension.

Worked Example 17.6

Question:

1. Show that $\gamma_{12} \sin \theta_1 = \gamma_{13} \sin \theta_2$ in Figure 17.12a.
2. If $\theta_1 = \theta_2 = 45°$ in Figure 17.12a, what is θ in Figure 17.12b?
3. What balances the vertical component of the tension $\gamma_{12} \sin \theta$ in Figure 17.12b? Ignore gravitational effects.

Answer:

1. At equilibrium the pressure throughout the system must be uniform. This implies that the Laplace pressures of the two interfaces are the same and that the curvature of each interface is uniform. The radii R_1 and R_2 of the upper and lower curved interfaces must therefore be related by $\gamma_{12}/R_1 = \gamma_{13}/R_2$. Since the radius of the three phase contact circle is

$r = R_1 \sin\theta_1 = R_2 \sin\theta_2$, we immediately obtain the desired result which shows that the resolved vertical components of the interfacial tensions are balanced, as expected.

2. Equating vertical components we have: $\gamma_{12}\sin\theta_1 = \gamma_{13}\sin\theta_2$. Equating horizontal components we obtain: $\gamma_{12}\cos\theta_1 + \gamma_{13}\cos\theta_2 = \gamma_{23}$ and $\gamma_{12}\cos\theta + \gamma_{13} = \gamma_{23}$. Eliminating γ_{12}, γ_{13} and γ_{23} from these three equations yields:

$$\cos\theta = \cos\theta_1 - (1 - \cos\theta_1)\sin\theta_1/\sin\theta_2. \tag{17.31}$$

Inserting $\theta_1 = \theta_2 = 45°$ into the above, we obtain $\theta = \cos^{-1}[\sqrt{2} - 1] = 65.5°$.

3. The apparently unbalanced vertical component of the tension $\gamma_{12}\sin\theta$ is balanced by high local stresses on the solid surface. This can result in elastic or even plastic deformations which cause the surface to bulge upwards (Shanahan and de Gennes, 1986), as illustrated in Figure 17.12c, left. More importantly, it may lead to molecular rearrangements that alter the local surface energies so as to reduce these local stresses (Figure 17.12c, right). These stress relaxation effects usually act to reduce the final contact angle below θ.

All the above effects can lead to hysteresis and aging effects of contact angles and adhesion energies. Thus, values of θ and W will usually differ for advancing and receding boundaries, with W_R being generally larger than W_A, so that $\theta_A > \theta_R$. As already mentioned, these differences also depend on dynamic factors such as the rate at which the boundaries move (see Section 17.8 and Chapter 18).

17.7 Adhesion of Solid Particles: the JKR and Hertz Theories

The adhesion force of two rigid (incompressible) macroscopic spheres is simply related to their work of adhesion by

$$F_{ad} = 2\pi\left(\frac{R_1 R_2}{R_1 + R_2}\right)W, \tag{17.32}$$

where $W = W_{132}$ in the general case of two different bodies 1 and 2 interacting in a third medium 3. This general result is a direct consequence of the Derjaguin approximation, Eq. (11.16), and leads to the following special cases:

for two identical spheres in liquid: $F = 2\pi R\gamma_{SL}$ (17.33a)

for two identical spheres in a vacuum: $F = 2\pi R\gamma_S$ (17.33b)

for a sphere on a flat surface in a vacuum: $F = 4\pi R\gamma_S$ (17.33c)

for a sphere on a flat surface in vapor: $F = 4\pi R\gamma_{SV}$ (17.33d)

Real particles, however, are never completely rigid as in Figure 17.13a, and on coming into contact, they deform elastically under the influence of any externally applied load as well as the attractive intersurface forces that pull the two surfaces together, which gives rise to a finite contact area even under zero external load (Figure 17.13b). One of the first

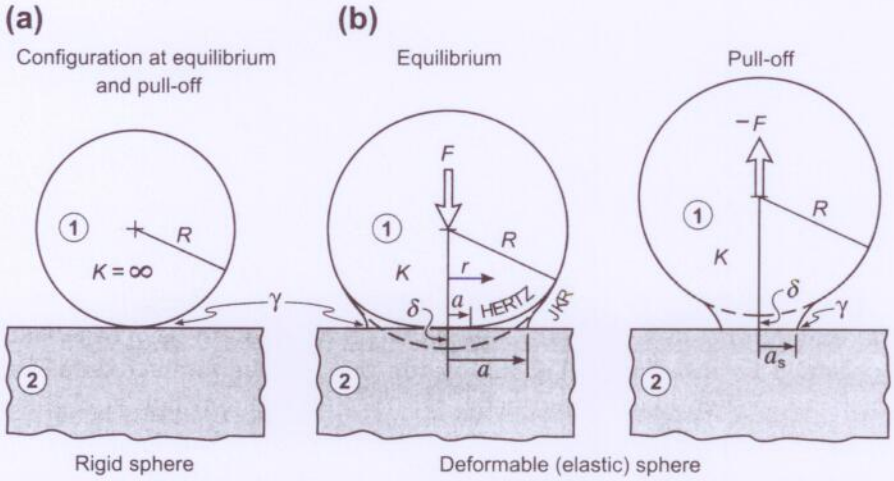

FIGURE 17.13 Hertz and JKR geometries of rigid and elastically deformable surfaces under external compressive (⇩) or tensile (⇧) loads *F*. **(a)** Rigid sphere on rigid surface. **(b)** Left: deformable (elastic) sphere on rigid surface in the absence (Hertz) and presence (JKR) of adhesion. **(b)** Right: elastic adhering sphere about to spontaneously separate from adhesive contact.

attempts at a rigorous theoretical treatment of the adhesion of elastic spheres is due to Johnson, Kendall and Roberts (1971), whose theory, the "JKR theory," forms the basis of modern theories of "adhesion mechanics" or "contact mechanics" (Johnson et al., 1971; Johnson, 1996; Pollock, 1978: Barquins and Maugis, 1982; see also Fig. 12.5). In the JKR theory two spheres of radii R_1 and R_2, elastic moduli K,[5] and surface energy W_{12} per unit area, will flatten when pressed together under an external load or force, F, such that at mechanical equilibrium their contact area will have a radius a given by

$$a^3 = \frac{R}{K}\left[F + 3\pi RW \pm \sqrt{6\pi RWF + (3\pi RW)^2}\right] \tag{17.34a}$$

$$= \frac{R}{K}\left(\sqrt{\frac{3}{2}\pi RW} \pm \sqrt{F + \frac{3}{2}\pi RW}\right)^2, \tag{17.34b}$$

where $R = R_1R_2/(R_1 + R_2)$. For a sphere of radius R on a flat surface of the same material (Figure 17.13b) we may put $R_2 = \infty$, $R = R_1$ and $W = 2\gamma_{sv}$ in the above equation, so that under zero load ($F = 0$) the contact radius is finite and given by

$$a_0 = (6\pi R^2 W/K)^{1/3} = (12\pi R^2\gamma_{sv}/K)^{1/3}. \tag{17.35}$$

The central displacement δ (see Figures 17.13b and c) is given by

$$\delta = \frac{a^2}{R}\left[1 - \frac{2}{3}\left(\frac{a_0}{a}\right)^{\frac{3}{2}}\right]. \tag{17.36}$$

[5]The elastic modulus K used here is related to E^* in Ken Johnson's classic book *Contact Mechanics* (Johnson, 1996 edition) by $K = 4E^*/3$.

Figure 17.14 shows how the contact area (a) and displacement (b) vary with the load. The load-displacement curve in Figure 17.14b may be thought of as the force-distance profile of the JKR interaction potential. Thus, if the sphere is pulled by a constant force F, it will detach from the surface when F reaches the "adhesion force" (also separation, detachment or pull-off force) given by:

$$F_{\text{ad}} = -\frac{3}{2}\pi RW = -3\pi R\gamma_{\text{sv}} \tag{17.37}$$

and separation will occur abruptly at a contact radius of $a_{\text{s}} = a_0/4^{1/3} = 0.63a_0$. Thus, from a measurement of the adhesion force F_{ad} one may determine the surface or interfacial energy or, more generally, the work of adhesion W_{132}. These values may also be obtained by measuring (Fig. 12.5) then plotting the contact radius a or area πa^2 against the applied load F, and using Eq. (17.34) to determine W if R and K are known.

The load-displacement or force-distance relationship of a JKR interaction is a subtle one. If the externally applied force is constant (e.g., a gravitational "dead weight" or buoyancy force), then detachment will occur at $F = F_{\text{ad}}$ and $a = a_{\text{s}}$ as given above. But if it is applied by a spring or compliant element, as is common in SFAs, AFMs, indenters, machines, and devices, detachment will occur when the slope of the force-distance curve in Figure 17.14 equals that of the force-measuring spring (see Figure 12.3). In particular, since the finite stiffness of the materials is an inherent part of the JKR interaction, the force-distance curves show instabilities even when measured with an infinitely rigid spring: a "jump-in" instability on the way in (from I to II) and a "jump-out" instability on the way out (from V to VI), which in other systems are determined by the stiffness of the external supporting structure or force-measuring spring.

Another useful equation of the JKR theory gives the pressure or stress distribution within the contact circle as

$$P(x) = \frac{3Ka}{2\pi R}(1-x^2)^{\frac{1}{2}} - \left(\frac{3KW_{12}}{2\pi a}\right)^{\frac{1}{2}}(1-x^2)^{-\frac{1}{2}}, \tag{17.38}$$

where $x = r/a$ (see Figure 17.13b). Equation (17.38) shows that inside a JKR contact the pressure is positive (compressive) near the center but tensile toward the edge, where theoretically it diverges, becoming infinite as $r \to a$ ($x \to 1$). The theory also predicts an infinite strain at the contact boundary, with each surface bending infinitely sharply through 90°. Indeed, material failure in the form of plastic deformations and microcracks is often observed at the boundary of an adhesive junction, brought about – not because the two materials are being pulled apart—but because of the enormous *equilibrium* negative stresses at the rim. Figure 17.15 shows a computer simulation of a metallic nano-junction showing some plastic deformation at the boundary but also surprisingly good agreement with the overall (elastic) deformation predicted by the JKR theory.

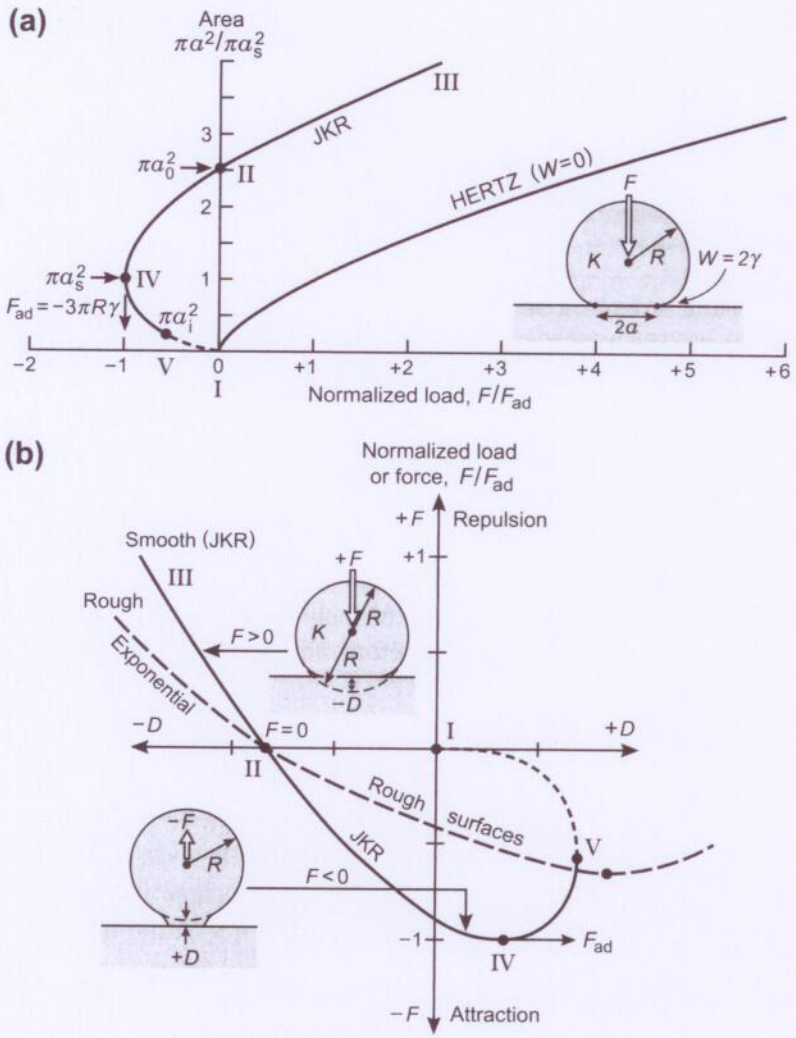

FIGURE 17.14 Need to add points I to V in both a and b. **(a)** Schematic "JKR plots" of the contact area versus load for adhering (JKR) and nonadhering (Hertzian) elastic spheres on a flat rigid surface, based on Eq. (17.34). **(b)** Effective JKR force-distance curve $F(D)$ for an elastic sphere on approach and separation from a rigid surface, where D is the same as the displacement δ in Figure 17.13b, given by Eq. (17.36), defined such that $D = \delta = 0$ at the point (I) when the sphere first touches the flat surface on approach (under no external force, $F = 0$) just before it spontaneously flattens and moves to point (II). Points (I) to (V) in (a) correspond to those in (b). The dashed curve in (b) illustrates the effect of roughness (Figure 17.17a).

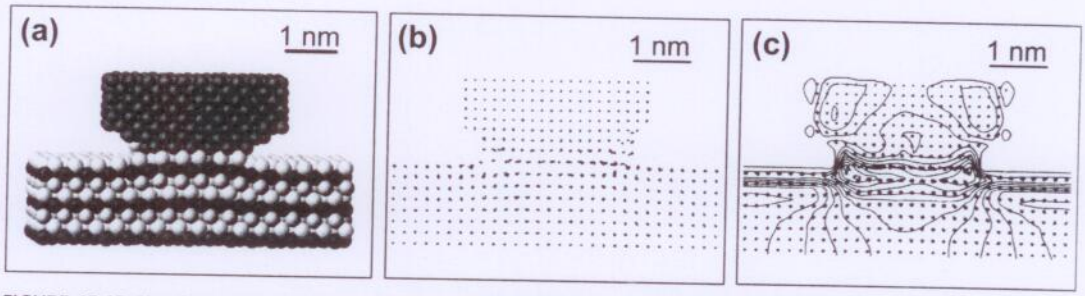

FIGURE 17.15 Simulation of an adhesive nano-junction between a nickel AFM tip and a (softer) gold surface just after the surfaces have jumped into contact, showing surprisingly good agreement with the JKR theory both for the mean positions of the atoms and the stress distribution, shown in **(c)**. The image is a snapshot averaged over ~1 ps. The fuzziness of some of the atoms in **(b)** reflect their higher mobility in regions where they are less confined. *[Adapted from Landman et al., (1990)* Science *248, 454–461.]*

It is interesting to note that, according to the JKR theory, a finite elastic modulus, K, while having an effect on the contact radius a or area πa^2, has no effect on the adhesion *force*, Eq. (17.37)—an interesting and unexpected result that has nevertheless been verified experimentally (Merrill et al., 1991; Mangipudi et al., 1994). On the other hand, the total adhesion *energy* of two elastically deformable surfaces in equilibrium contact (at $F = 0$) is given by (Johnson, 1985)

$$E_0 = -0.6\pi a_0^2 W = -1.2\pi a_0^2 \gamma \tag{17.39}$$

which *does* depend on the modulus K via Eq. (17.35)—the lower the modulus K the higher the adhesion energy. This energy is 40% smaller than the purely surface energy needed to separate the two particles of equilibrium contact area πa_0^2 because of the additional positive (unfavorable) elastic energy stored in the system. Table 17.2 gives the K values of some common materials. Note the 11 orders of magnitude variation as we go from the hardest materials (e.g., diamond) to the softest (biological cells).

As elaborated in Section 17.2, the adhesion force provides information on the force that must be applied to spontaneously detach a particle from another—an essentially nonequilibrium process. In contrast, the energy tells us more about the equilibrium thermodynamic state of a system of particles, such as the probability of finding the particles dispersed or in contact (aggregated), and the mean lifetimes or spontaneous on- and off-rates of the particles in the absence of any external pulling force. Such issues become more important for smaller particles, such as nanoparticles, biological macromolecules and vesicles, where the interaction energies are often comparable to kT and where lifetimes fall in the range of "engineering interest" or "everyday experience" (Table 9.1): nanoseconds ($\sim 10^{-9}$ s) to many years ($\sim 10^{+9}$ s).[6]

[6]Since lifetimes are proportional to $e^{-E_0/kT}$ an order of magnitude change in E_0—say, from $4kT$ to $40kT$—will lead to a change in the lifetime of a bond or adhesive junction of more than 15 orders of magnitude.

Table 17.2 Young's Modulus (Y = Stress/Strain) of Some Common Materials

Nonbiological Materials (MPa)[a,b]		Biological Materials and Tissues (MPa)[a]	
Weak gels	<1[c]	Brain matter	0.0005 (500 Pa)
Soft rubber	1–10	Cells	0.001–0.1
Hard rubber	100	Fluid lipid bilayers	50
Soft polymers (nylon, Teflon, PE)	500	Gel state bilayers	200
Hard polymers (PMMA, PS, PVC)	3,000	Soft, spongy bone	100
Soft metals (Mg, Al), glass	40,000–80,000	Protein crystals	100–1,000
Hard metals (bronze, steel, Ti)	100,000–200,000	Microtubules, virus capsids[d]	1,000
SiC, WC, diamond	450,000–1,100,000	Hard bone, enamel	20,000–50,000

[a]1 MPa = 10^6 N m^{-2} = 145.0 psi (lb/in^2).

[b]See Table 16.1 for full polymer names.

[c]Gels, aerogels, and foams can be as dense and stiff as a microstructured ceramic or so open and frail that they cannot hold their own weight (K < 1 kPa).

[d]Layered materials composed of molecularly thin (2D) sheets have different Young's moduli in different directions. For example, graphene—the single molecule-thick sheet of single-walled microtubules and graphite—has a Young's modulus of 10^{12} Pa in the plane of the monolayer (Lee et al., 2008), which is the same as for diamond: the covalent C–C bonds are essentially the same in these three structures. In contrast, the Young's modulus of graphite in the direction normal to the layers, which are held together by van der Waals forces, is ~10^{10} Pa. If one can talk about the Young's modulus in 1D, then an alkane chain also has a Young's modulus of ~10^{12} Pa (Akhmatov, 1966).

Worked Example 17.7

Question: Two spherical metal particles of radius 0.1 mm, elastic modulus $K = 10^{11}$ N m^{-2} and surface energy $\gamma = 1.0$ J m^{-2} are in adhesive contact under zero external force. What is the compressive pressure between them at the center of the contact circle? The tensile strength of the material is 250 MPa. How far in from the boundary will the material fail? What will change with time if the particles are allowed to remain in contact indefinitely?

Answer: For two spheres of equal radii $R_1 = R_2 = 0.1$ mm, we may insert $R = 0.05$ mm and $W = 2\gamma = 2.0$ J m^{-2} in the JKR equations. Since $F = 0$, the radius of the contact circle is $a = a_0 = (6\pi R^2 W/K)^{1/3} = 9.8 \times 10^{-7}$ m (0.98 μm). Using Eq. (17.38), the pressure at the center ($x = r/a = 0$) is therefore:

$$P(0) = (3Ka_0/2\pi R) - (3KW/2\pi a_0)^{\frac{1}{2}} = +(6K^2W/\pi^2R)^{1/3}. \tag{17.40}$$

Inserting the above values for K, W, and R we obtain a positive (compressive) pressure of $P(0) = 6.24 \times 10^8$ N m^{-2} (~600 MPa or ~6,000 atm). With increasing radial distance r from the center the pressure changes from compressive to tensile at $x = 0.82$, and reaches a value equal to the tensile strength at $x = 0.88$, which corresponds to $r = 0.88a_0 = 0.88 \times 0.98 = 0.87$ μm, which is 110 nm from the boundary. Thus, tensile failure is expected to occur within this region, manifested by submicron cracks or plastic deformation (material flow) to relax the elastic stresses at the boundary.

At finite temperatures all materials are viscoelastic and will flow or creep, however slowly.[7] Thus, with time, the adhering particles will deform to minimize the total surface and interfacial

energy. If the two metals are of the same material they will slowly coalesce (cold-weld): the interface will disappear and the two truncated spheres will slowly deform by bulk creep and/or surface diffusion[8] until they form a single sphere or, if the materials are crystalline, a single facetted crystal. If the materials are different the interface will not disappear but the spheres will still deform until one material engulfs the other or they form a doublet, similar to two adhering soap bubbles. The final shapes of the particles will depend on the crystal structure and surface and interfacial energies of the different crystallographic faces of the two metals.

[7]See the fascinating *Pitch Drop Experiment* website, perhaps the longest ongoing experiment in history.
[8]Particle shape changes via surface diffusion occur much faster for smaller particles. Since the time to diffuse a distance x is proportional to x^2, a (nano)particle with an initial radius of 10 nm will deform by surface diffusion 10^{10} times faster than one with a radius of 1 mm (see Section 11.4).

The Hertzian limit. For nonadhering surfaces ($W = 0$, $\gamma = 0$), as well as for very high loads ($L \gg L_{ad}$), all the equations of the JKR theory reduce to those of the earlier Hertz theory for nonadhering elastic spheres (Hertz, 1881; Johnson, 1985):

$$\text{Adhesion force and energy:} \quad F_{ad} = 0, E_0 = 0 \tag{17.41a}$$

$$\text{Contact radius:} \quad a^3 = RF/K \tag{17.41b}$$

$$\text{Displacement:} \quad \delta = a^2/R = F/Ka \tag{17.41c}$$

$$\text{Pressure:} \quad P(x) = 3Ka(1-x^2)^{\frac{1}{2}}/2\pi R = 3F(1-x^2)^{\frac{1}{2}}/2\pi a^2. \tag{17.41d}$$

The last equation shows that the pressure is zero at the edge ($x = 1$, $r = a$) and maximally compressive at the center ($x = r = 0$), where $P(0) = \frac{3}{2} F/\pi a^2$, which is 1.5 times the mean pressure across the contact circle. Unlike the situation in a JKR contact where the stress is (theoretically) infinite at the boundary, it is zero at the boundary of a Hertzian contact.

Apart from its breakdown within the last few nanometers of the bifurcation boundary, most of the equations of the JKR theory and all the equations of the Hertz theory have been experimentally tested for molecularly smooth surfaces and found to apply extremely well even at the submicron scale (see Figure 17.15 and Horn et al., 1987; Bhushan, 1995; Landman et al., 1990; Luedke and Landman, 1992; Carpick et al., 1996a, b; McGuiggan et al., 2007).

In the following sections we shall investigate other common situations where the JKR theory breaks down or no longer applies. These involve systems where the surface energy changes with time, where the materials are viscoelastic (rather than elastic), and when surfaces are not smooth, all of which can give rise to hysteresis and time-dependent effects.

17.8 Adhesion Hysteresis

Just as in the case of a liquid droplet advancing or receding on a surface, a growing (advancing) and contracting (receding) contact area between two solid surfaces can also

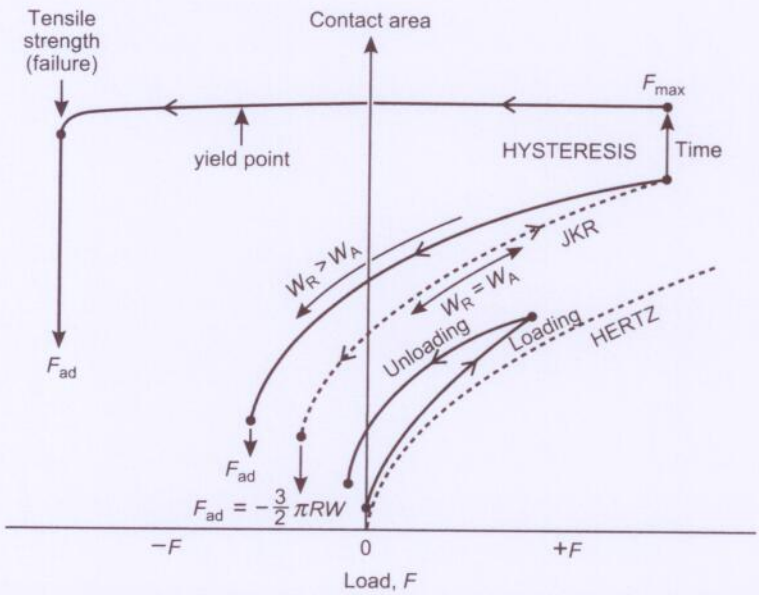

FIGURE 17.16 "JKR-plots" showing reversible and irreversible or "hysteretic" loading-unloading "JKR cycles" and "Hertz cycles." Dashed curves show reversible paths; solid curves show hysteretic paths. In practice, W, R, and/or K can change with the contact time and loading-unloading rates. When these changes are large (compared to the initial values on loading) the unloading curve is no longer described by Eq. (17.34). For example, if two viscoelastic materials are allowed to remain in contact for a long time after loading, their contact area will increase even at constant load. They may also partially coalesce (increasing W), and if they are then separated quickly, the unloading path will correspond to that of a solid undergoing brittle or ductile failure, as shown in the top curve.

have different values for W or γ, referred to as W_A and W_R, giving rise to adhesion energy hysteresis (Figure 17.16) which is entirely analogous to contact angle hysteresis (Figure 17.11). With polymeric materials this effect arises because of chain interdigitations occurring across the contact interface that increase the effective contact area (or number of interfacial bonds) as a function of time (Figure 17.17b). With metals and inorganic solids such as silica, the effect can be due to slow coalescence or chemical sintering reactions (Figure 17.18). Both of these effects give rise to an adhesion energy on loading (coming on or advancing), W_A, that is less than the energy on unloading (coming off or receding), W_R, and thus to hysteresis effects and energy dissipation during a JKR loading-unloading cycle (see Figure 17.16).

Even the simplest adhesion processes are unlikely to be reversible, but involve energy dissipation,[9] having profound effects for understanding why things actually stick together after they come into contact, and providing a link between adhesion and friction (Chapter 18). For example, if a body is attracted to a surface via a Lennard-Jones type

[9]As previously mentioned, "energy dissipation" is a misnomer, since energy is never dissipated in the sense of being "lost"; rather, it is converted into a different form. In this case, mechanical or kinetic energy is converted into heat.

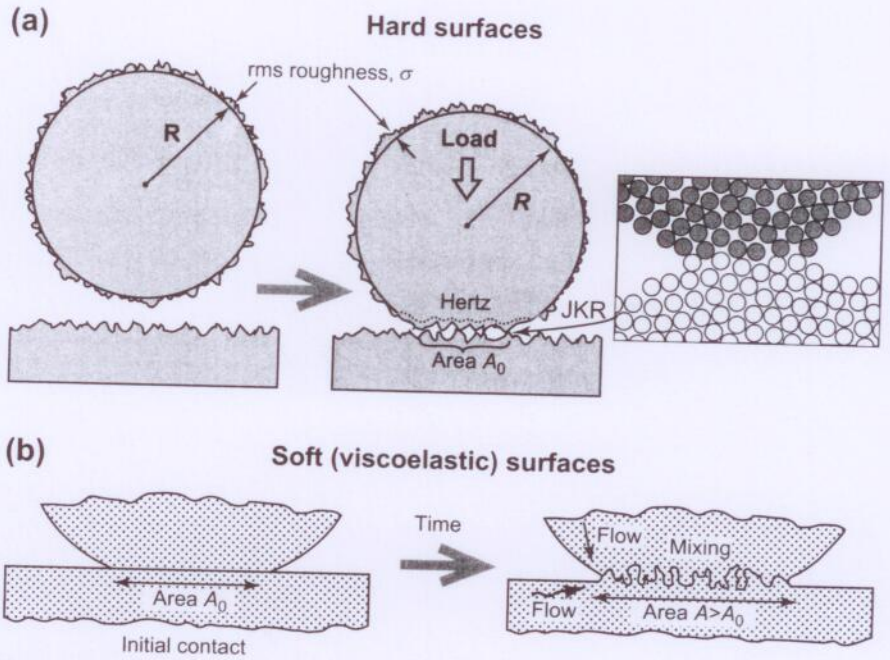

FIGURE 17.17 Examples of rough contacts and aging effects at hard and soft adhesion junctions. **(a)** Hard elastic materials exhibit lower adhesion forces than predicted by the JKR theory since the real (total molecular) area of contact is less than that predicted by the JKR theory, A_0. Local junctions can be JKR-like, as in Figure 17.15, at the same time as the mean overall shape is closer to Hertzian. **(b)** The surfaces of soft and viscoelastic materials deform on coming into adhesive contact so that the real contact area A can exceed the JKR area, A_0. The molecules of viscoelastic materials interpenetrate (mix) across the interface and flow with time resulting in time-dependent (aging) effects, manifested by a progressive increase in both the real (molecular) contact area and the apparent (projected) area and enhanced adhesion forces that can be as much as 10^4 higher than predicted by the JKR theory (which may be compared with the *reduction* in F_{ad} in the case of hard rough surfaces). If the two surfaces are different (immiscible), the interdigitation will saturate; if they are the same, it will continue to completion—that is, until there is no more interface between the now continuous material.

potential, one would think that if it is allowed to approach that surface it would stick to it. However, under ideal reversible conditions, it would simply bounce back at the same velocity $(-V)$ as its original approach velocity $(+V)$. If its kinetic or thermal energy is to change, some "energy transfer" or "internal friction" mechanism has to be operating (cf. Sections 2.10, 9.3 and Chapter 18), whereby the body ends up in the bottom of the potential well and the temperature of the surface, body, and surroundings has increased. Even the "jumps-into-contact," as commonly seen and used to measure attractive forces, would not occur in the absence of an energy transfer mechanism. Since this issue forms the basis of understanding friction, further discussion on adhesion and surface energy hysteresis, and its intimate relationship to friction, is deferred to Chapter 18.

Another effect that gives rise to adhesion hysteresis in JKR plots is viscoelasticity of the material—that is, in K, which always has both a real (static elastic) and imaginary

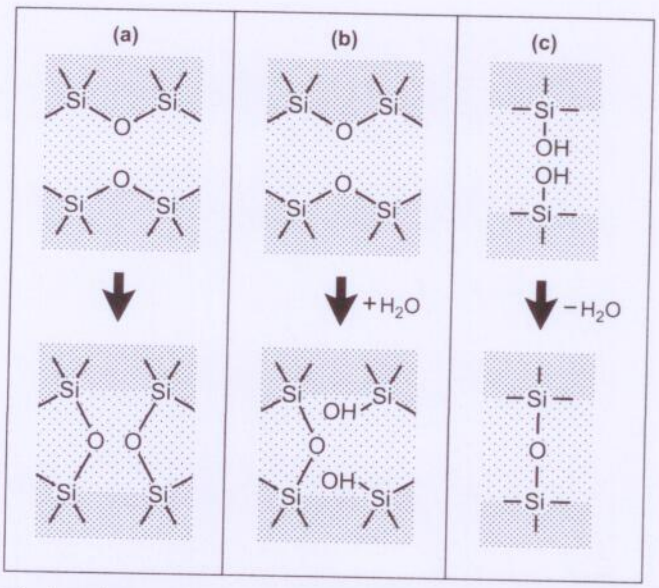

FIGURE 17.18 Slow chemical reactions can increase the adhesion of particles with time through the formation of covalent bonds. The examples show the sintering of silica or quartz (SiO_2) surfaces, in each case resulting in strong siloxane (Si-O-Si) across the interface, which eventually disappears. Such reactions may occur naturally **(a)**, but they often involve the uptake of water from the atmosphere **(b)** or loss of water **(c)**.

(dynamic energy dissipating) part, denoted by $G'$and G'' (Ferry, 1980).[10] Viscoelastic junctions deform with the time they are left in contact (Figure 17.17b) and with the loading and unloading rates, both of which affect the JKR loading and unloading paths, as illustrated in Figure 17.16. It is often difficult to distinguish between an enhanced adhesion that is due to molecular interdigitation or sintering at the interface without an increase in the "apparent" (projected or macroscopic) contact area, and one due to bulk viscous flow that does increase the contact area.

Worked Example 17.8

Question: According to the JKR theory, the adhesion force needed to separate an elastic sphere from a flat surface is $\frac{3}{2}\pi RW$. Derive an approximate expression for the pull-off force when the materials are viscoelastic (as are many types of polymers) and where the separation is done very rapidly. What are the two adhesion forces for each of the above conditions when $R = 1$ cm, $W = 100$ mJ m^{-2}, and the "quasi-static" value of K is 100 MPa?

Answer: In the limit of very rapid separation the surfaces do not have time to deform from their equilibrium shape (at $F = 0$) and therefore come apart while maintaining this geometry. Thus, the surfaces will separate not by peeling away from each other, which is implicit in a

[10]Strictly, K and G are different, being related by $G = Kf(\nu)$, where ν is the Poisson ratio whose typical value is 0.3.

JKR-type separation, but with the contact circle remaining in the planar geometry with a constant area of $\pi a_0^2 = \pi(6\pi R^2 W/K)^{2/3}$. The pull-off force for this type of separation is $F_{ad} = \pi a_0^2 W/D_0 = \pi(6\pi R^2 W^{5/2}/K)^{2/3}/D_0$, where $D_0 \approx 0.2$ nm is the effective range of the molecular forces. This adhesion force increases as K decreases even as the JKR force, $\frac{3}{2}\pi RW$, remains unchanged. Inserting the given values, we obtain $\frac{3}{2}\pi RW = 4.7$ mN, and $\pi a_0^2 W/D_0 = 24.0$ N, which is approximately 5,000 times larger.[11]

[11] It is for this reason that it is wise to peel away adhesive tape from paper slowly rather than quickly if you don't want to remove some of the paper as well.

Stick-slip adhesion. When two surfaces are separated from adhesive contact, either by peeling as in Figure 17.2b or through a JKR-type unloading path (Figure 17.16), even if the pulling force is increased at a steady rate the contact area may decrease in a "stick-slip" fashion. A similar effect can occur when a liquid boundary advances: sticking then slipping to the next sticking or "pinning" point, then slipping again. The sticking and slipping states are often described as the "static" and "kinetic" regimes of motion, but they actually represent regimes having finite but very different rates of motion—one very slow, the other very fast. The reasons for stick-slip adhesion and other types of forces showing "intermittent" behavior are explored in detail in the following chapter on friction and lubrication forces.

17.9 Adhesion of Rough and Textured Surfaces

The JKR and Hertz theories assume perfectly smooth surfaces. Most surfaces are rough or "textured," and asperities as small as 1–2 nm can significantly lower their adhesion (Persson, 2000), but roughness can also increase the adhesion. Roughness and texture can come in many guises: surface asperities can be randomly rough or fractal, have uniform height but variable widths or uniform widths but variable heights, have a periodic pattern, and so on. For this reason there is as yet no general mathematical way of defining roughness (or surface topography) that covers all possible situations. In Section 17.5 we saw how texture can affect the wetting properties of surfaces, giving rise to very complex phenomena. Here we shall look at how different types of surface texture can affect their adhesion.

Figure 17.17a shows the deformations of a rough adhesive junction of RMS roughness σ. Locally, each asperity-asperity contact may be treated as a small JKR junction with a much smaller radius than the macroscopic particle radius R. The total adhesion force is therefore much smaller than the JKR adhesion force for the smooth surfaces ($\sigma = 0$). A schematic JKR force-distance curve for rough elastic particle surface is illustrated by the dashed line in Figure 17.14b. Recent experiments (Benz et al., 2006; Zappone et al., 2007) and modeling (Yang et al., 2008) suggest that the adhesion force decays exponentially with the roughness σ according to

$$F_{ad}(\sigma) = F_{ad}(0)e^{-\sigma/\sigma_0}, \tag{17.42}$$

where σ_0 is a constant and $F_{ad}(0)$ is the JKR adhesion force for smooth surfaces ($\sigma = 0$), and that the repulsive part becomes exponential rather than being described by Eqs (17.34) and (17.36). Since the net adhesion force of a rough junction is low, the mean overall (macroscopic) deformation of the junction closely follows a Hertzian shape even though the local micro- and nano-contacts are JKR-like (cf. Figure 17.17a). It has also been found that the repulsive parts of the loading-unloading curves of rough surfaces can be hysteretic, as illustrated in Figure 17.16. This effect can arise even when the surfaces and the asperities themselves are not deformed plastically (Section 17.10), and appears to be a consequence of having more contacts "on the way out" than "on the way in"—a situation that does not arise with a single asperity junction.

In contrast to the generally low adhesion of rough *elastic* surfaces, *viscoelastic* materials will flow once they come into adhesive contact so that the real contact area, or number of adhesive bonds at the interface, will increase with time until it *exceeds* the value for smooth surfaces, as illustrated in Figure 17.17b. In this case the initial roughness profile is completely lost soon after the surfaces come into contact, making the adhesion force larger rather than smaller than the ideal JKR value. In general, both molecular-level mixing and chemical bonding across the interface (interdigitation, interdiffusion, reptation, sintering, coalescence, cold welding), and bulk flow at the boundaries (viscous creep) can occur.

17.10 Plastic Deformations

The mechanical properties of viscoelastic and other types of nonelastic materials is outside the scope of this book, but the salient differences in the *contact mechanics* and *adhesion mechanics* of plastic and elastic solids will now be briefly described. At high loads, materials no longer deform elastically: deformations are no longer proportional to the applied load or reversible on releasing the load. The atoms or molecules "flow," but the flow is unlike the flow in a liquid: it stops as soon as the load or stress is removed, as illustrated in Figures 17.19a and b for a compressive load. The *yield stress* (also *flow stress*) P_Y defines the transition or *yield point* from elastic to *plastic* (also *ductile*) behavior, where the strain no longer varies linearly with the applied pressure P—that is, where the elastic modulus is no longer constant (Figure 17.19c).

Complete *failure* or *fracture* of the material—for example, a material breaking into two parts on being stretched or sheared—occurs at the *failure* or *fracture strength* of the material. The yield stresses, and especially failure stresses, of nonelastic materials can be very different on compression and tension. For example, no material can be compressed beyond a strain of -1; however, some fibers may be stretched to many times their original length (strain $\gg 1$) before they finally snap. For these reasons the deformations (displacements), forces, and various yield points on loading (compression) and unloading (tension) are usually quite different, requiring these phenomena to be considered separately. Loading phenomena include indentation; unloading

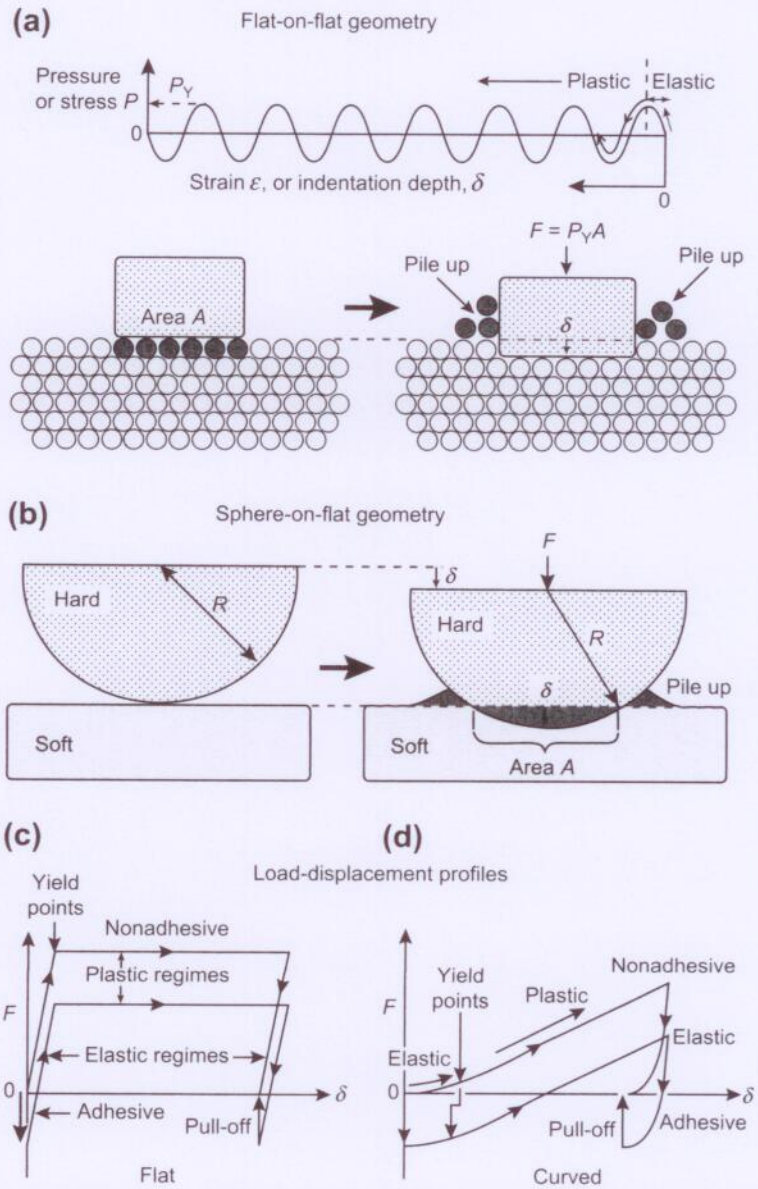

FIGURE 17.19 Deformations and associated forces of plastically deforming solids of different geometries. **(a)** Idealized pressure-distance curve when a crystal is compressed: after the initial elastic regime, atomic layers get pushed out, ideally one at a time, so long as the applied pressure is kept at the yield stress P_Y. The schematics show six extruded atoms that have piled up at the edges; these no longer contribute to the pressure. Panel **(c)** shows the load-displacement paths on loading and unloading for the flat-punch geometry for nonadhesive and adhesive contacts. Note that on unloading, the materials relax elastically before finally detaching (pull-off). Panels **(b)** and **(d)** show the same features for the sphere-on-flat geometry or between any two curved surfaces.

phenomena include extensive stretching or abrupt cracking failure (for brittle materials), and most of these processes involve nonequilibrium time-dependent "aging effects" such as creep.

Bodies under compression. Figure 17.19 illustrates the origin of plasticity, the transition from elastic to plastic flow, and why the "flow" stops or relaxes when the compressive stress is removed. The load-displacement curves are hysteretic (irreversible), which is quite different from those of elastically deforming bodies, described by the JKR theory (compare Figures 17.19c and d with Figure 17.14b). Two common geometries used in compression or indentation measurements are the "flat punch" and "round punch" geometries, where the punch is hard and is assumed not to deform as the softer material plastically deforms.

As shown in Figure 17.19c, for the *flat punch* geometry the elastic regime, where $P(\delta) \propto \delta$, is followed by the plastic regime, where $P = F/A = P_Y$ = constant. The corresponding forces for the *round punch* geometry can be readily determined from the flat punch equations using the Derjaguin approximation, Eq. (11.16). Thus, for the elastic regime we obtain $F(\delta) = 2\pi RE(\delta) = 2\pi R\int P(\delta)d\delta \propto 2\pi R\delta^2$, and for the plastic regime we obtain $F(\delta) = 2\pi R\int P_Y d\delta = 2\pi RP_Y\delta + C$, where C is a constant determined by the extent of the elastic regime (see Problem 17.22). Thus, in the initial "elastic" regime we expect $F \propto \delta^2$ while in the plastic regime $F \propto \delta$, as illustrated in Figure 17.19d, and seen in most indentation measurements (Johnson, 1985; Oliver and Pharr, 1992). More recent nano-indentation measurements have revealed some of the discreteness (stick-slip) effects expected at the atomic scale (Cross et al., 2006).

For small deformations ($\delta \ll R$) and constant R, the chord theorem, Eq. (10.4), allows us to further simplify the above equation to give, in the plastic regime:

$$F(\delta) = 2\pi RP_Y\delta + \text{const.} = P_YA + \text{const.} \tag{17.43a}$$

or, for small C,

$$P_Y = F(\delta)/A. \tag{17.43b}$$

Thus, the permanently deformed area A is proportional to the load only—that is, independent of the indentation depth δ or radius R of the punch or ball. This relationship forms the basis of various methods to measure the *hardness* H of materials, which is defined by an equation similar to Eq. (17.43b)—for example, $H \propto$ load/area—where the area may be the actual or projected surface area of the indentation and where H is proportional to, but not the same as, the elastic limit or yield stress (Maugis & Pollock, 1984).

The loading-unloading paths of plastically deforming bodies are hysteretic, but in a different ways from the hysteresis observed with rough elastic surfaces. In the latter case, the hysteresis is reversible on repeated loading-unloading cycles, while in the former it is not.

Bodies under tension. The situation of bodies under tension is much more complex. The unloading curves of Figures 17.19c and d, showing abrupt JKR-like detachment (pull-off) assume that the contact interface remains intact—that is, that the two surfaces have

not merged or coalesced. When there is full or partial coalescence, the junction ruptures or fractures, but the rupture mechanism depends on the geometry, the viscoelastic properties of the material, and the separation rate or force, and can involve stringing, fibrillation, Saffman-Taylor fingering and internal cavitation. The effective adhesion forces and energies can be 3 to 4 orders of magnitude higher than the ideal values for elastic solids—for example, $F_{ad} = 3\pi R\gamma_S$ for a sphere on flat geometry.

17.11 Capillary Forces

The mechanical and adhesive properties of many substances are very sensitive to the presence of even trace amounts of "condensable" vapors in the atmosphere—that is, vapors whose liquids form a small contact angle with the surface. For example, the stability of colloids in organic liquids, the adhesion of powders and sand (granular materials), the seismic properties of rocks, and the swelling of certain polymers into gels are markedly dependent on the relative humidity. All these effects are due in part to the *capillary condensation* of water at surface contact sites (e.g., in cracks, pores and hydrophilic molecular groups), which, as we shall see, can have a profound effect on the adhesion strength[12] of junctions, both large and small.

Liquids that wet or have a small contact angle on surfaces will spontaneously condense from vapor into cracks and pores (Figure 17.20a, b). At thermodynamic equilibrium the curvature of a concave meniscus (or convex droplet) surface $(1/r_1 + 1/r_2)$ is related to the relative vapor pressure (relative humidity for water) by the Kelvin equation. The Kelvin equation can be derived from the general equation, Eq. (13.26), relating pressure to the relative vapor pressure: $P = (kT/v)\log(p/p_{sat}) = (RT/V)\log(p/p_{sat})$, where v and V are the molecular and molar volumes, respectively, p the vapor pressure and p_{sat} the saturated vapor pressure. Equating P with the Laplace pressure, Eq. (17.15), we immediately obtain the *Kelvin equation*

$$r_K = \left(\frac{1}{r_1} + \frac{1}{r_2}\right)^{-1} = \frac{\gamma V}{RT\log(p/p_{sat})}, \tag{17.44}$$

where r_K is the *Kelvin radius*. For water at 20°C, $\gamma V/RT = 0.54$ nm. Thus, for a spherical concave water meniscus (putting $r_1 = r_2 = r$), we find $r_K = \infty$ at $p/p_{sat} = 1.0$ (saturated vapor), $r_K \approx -5.1$ nm at $p/p_{sat} = 0.9$, $r_K \approx -0.8$ nm at $p/p_{sat} = 0.5$, and $r_K \approx -0.23$ nm at $p/p_{sat} = 0.1$ (10% relative humidity).

What is the effect of a liquid condensate on the adhesion force between a macroscopic sphere and a surface (Figure 17.20c)? A simple derivation is to consider the *Laplace pressure* in the liquid: $P_L = \gamma_L(1/r_1 + 1/r_2) \approx \gamma_L/r_1$, since $r_2 \gg r_1$. The Laplace pressure acts on an area $\pi x^2 \approx 2\pi Rd$ between the two surfaces, thus pulling them together with

[12]The commonly used term *adhesion strength*, like *bond strength*, is not recommended, since it is not clear whether it refers to the force or energy of the contact, which, as discussed in Sect. 17.2, are qualitatively different both in their units and the effects they give rise to.

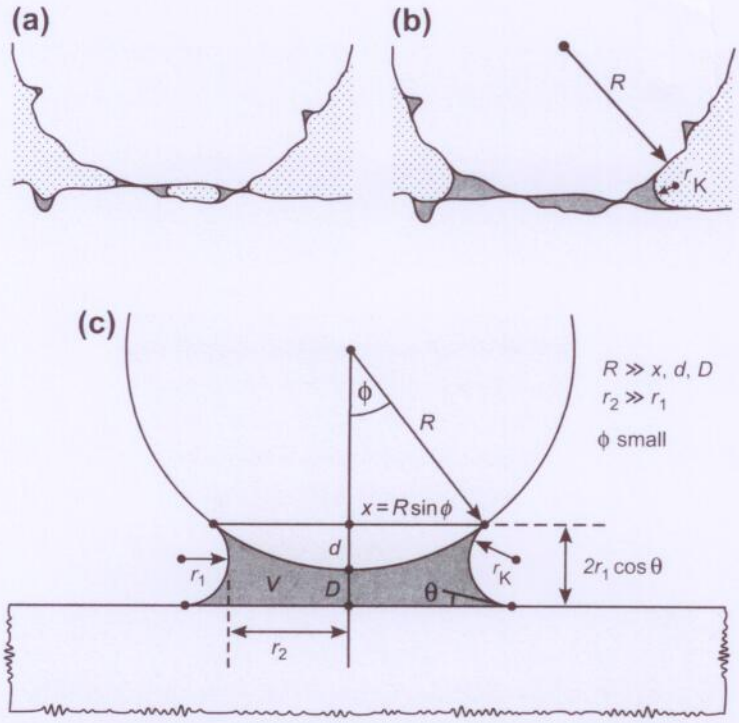

FIGURE 17.20 **(a)** and **(b)**. Capillary condensation of liquids at contact junctions and in pores and cracks. The concave menisci formed give rise to a tensile Laplace pressure within the liquid which gets transmitted to the surrounding solid(s) causing particles to attract each other and pores and cracks to close. However, if the direct inter-surface force is repulsive in the liquid, the short range force will be repulsive which can cause microcracks to open rather than close. **(c)** Geometry of capillary bridge between a sphere and a flat. If the condensate is in thermodynamic equilibrium with the surrounding vapor, its mean radius of curvature is the *Kelvin radius*. In saturated vapor, condensation will continue until the liquid surface has zero mean curvature ($r_2 = -r_1$ everywhere); such a surface can be flat (planar) or a *minimal surface* (see Problem 17.19).

a force $F \approx -2\pi R d\gamma_L / r_1$. For small ϕ, $(d + D) \approx 2r_1 \cos\theta$, and we can express the Laplace pressure contribution to the adhesion force as

$$F(D) = -4\pi R\gamma_L \cos\theta\left(1 - \frac{D}{2r_1 \cos\theta}\right), \tag{17.45a}$$

or, equivalently,

$$F(D) = -\frac{4\pi R\gamma_L \cos\theta}{(1 + D/d)}. \tag{17.45b}$$

The additional force arising from the resolved normal surface tension around the circumference, $\sim 2\pi x\gamma_L \sin\theta$, is always small compared to the Laplace pressure contribution except for $\theta \approx 90^\circ$ when $\cos\theta \approx 0$ and $\sin\theta \approx 1$.

Worked Example 17.9

Question: A cylindrical liquid bridge of constant volume V and radius R is held by capillary forces between two hydrophobic surfaces (where $\theta = 90^\circ$) as shown in Figure 17.21. Calculate the normal force F between the two walls using two different methods: (1) by resolving forces, and (2) by considering the surface energies γ_L, γ_S, and γ_{SL} of the various surfaces and interfaces. You should, of course, arrive at the same result in each case. Ignore gravitational effects.

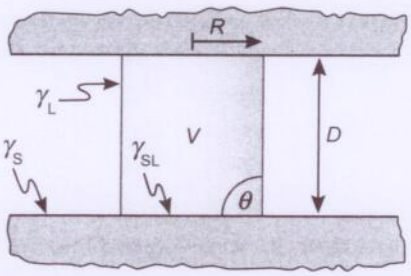

FIGURE 17.21 Liquid capillary bridge of constant volume $V = \pi R^2 D$ and contact angle $\theta = 90^\circ$. On increasing D liquid bridges become unstable and snap at the critical separation $D = D_c = 2\pi R = (4\pi V)^{1/3} \propto V^{1/3}$.

Answer: (1) Resolving the forces in the normal direction, we first have the compressive Laplace pressure acting on the surfaces by the liquid, giving rise to a (repulsive) force between them of $P_L \times \text{area} = (\gamma_L/R) \times (\pi R^2) = +\pi R \gamma_L$. The normally resolved surface tension force of $\gamma_L \cos\theta = \gamma_L$ per unit length acting along the circumference of length $2\pi R$ gives rise to an additional force at the boundary of $-2\pi R\gamma_L$. The total force is therefore

$$F(D) = -\pi R\gamma_L = -\gamma_L\sqrt{\pi V/D}\ (\text{since } V = \pi R^2 D = \text{constant}). \tag{17.46}$$

Thus, the net force is attractive—pulling the surfaces together and varying as $1/D^{1/2}$.

(2) Since the contact angle is $\theta = 90^\circ$, the Young Equation, Eq. 17.24, tells us that $\gamma_{SL} = \gamma_S$. If A is the (constant) *total* area of each flat surface, the total surface energy of the system is $E = 2\pi RD\gamma_L + 2\pi R^2\gamma_{SL} + (2A - 2\pi R^2)\gamma_S = 2\pi RD\gamma_L + 2A\gamma_S$. Expressing E in terms of D and the constant volume V gives, $E = 2\gamma_L\sqrt{\pi VD} + 2A\gamma_S$, which on differentiating with respect to D gives Eq. (17.46).

Equation 17.45 shows that for a sphere and a flat surface the maximum capillary force occurs at contact, when $D = 0$, and is given by

$$F(D = 0) = F_{ad} = 4\pi R\gamma_L \cos\theta. \tag{17.47}$$

For surfaces with different contact angles, θ_1 and θ_2, it is easy to show that the adhesion force is

$$F_{ad} = 2\pi R\gamma_L(\cos\theta_1 + \cos\theta_2). \tag{17.48}$$

The two forms of Eq. 17.45, although equivalent, apply to two quite different situations where the capillary forces vary differently with D even though the values at $D = 0$ are the same. The two situations correspond to those of thermodynamic equilibrium and constant liquid volume. In the first, the liquid bridge is at equilibrium with the vapor so that the mean curvature of the meniscus remains constant as D changes (via evaporation or condensation) and equal to the Kelvin radius, r_K—that is, $r_1 \approx r_K$ in Figure 17.20c. Since θ is also constant, Eq. (17.45a) applies, showing that the force-distance function is a straight line that cuts the $F = 0$ axis at $D = 2r_K \cos\theta$, at which separation the bridge finally disappears (see Problem 17.10). In the second scenario, the liquid is "involatile" or effectively of constant volume during the separation of the surfaces. Equation 17.45b now becomes more convenient, where $(d + D)$ is no longer constant but a function of V, R, D and θ. The attractive force is now longer-ranged, and at some separation D (proportional to $V^{1/3}$) a spontaneous Raleigh-like snap-off occurs (see Problem 17.2 and Willett et al., 2000).

A rigorous analysis of the meniscus shape and capillary force of even the simplest geometry is actually quite complicated. First, the liquid surface must have the same Laplace pressure and therefore the same mean curvature $(1/r_1 + 1/r_2)$ throughout, and so in the case of the liquid neck just discussed cannot be circular, as indicated by the concave radius r_1 in Figure 17.20c, since the orthogonal radius r_2 cannot also be constant. Surfaces of constant mean curvature everywhere are known as *minimal surfaces*. The shape of the meniscus must also satisfy the boundary condition(s) of constant contact angle(s) at all points on the two surface(s) irrespective of their geometry.[13] In the case of the capillary bridges between spheres and/or planar surfaces, more rigorous expressions, valid for large ϕ and different contact angles on each surface, have been derived by Orr et al., (1975).

One other important parameter must be included in the above expressions. This is the direct solid-solid contact adhesion force inside the liquid annulus, Eq (17.33). For a sphere and a flat surface the final result is therefore

$$F_{ad} = 4\pi R(\gamma_L \cos\theta + \gamma_{SL}) = 4\pi R\gamma_{SV}. \tag{17.49}$$

Fogden and White (1990) and Maugis and Gauthier-Manual (1994) considered the effects of JKR-type deformations on capillary forces and concluded that for strong solid-solid adhesion Eq. (17.49) becomes: $F_{ad} = 4\pi R(\gamma_L \cos\theta + 0.75\gamma_{SL})$, while if the meniscus radius is very small it becomes $F_{ad} = 3\pi R(\gamma_L \cos\theta + \gamma_{SL})$. Note, however, that if the solid-solid interaction in the liquid is short-range repulsive, this additional contribution will be negative and D will be finite at "contact equilibrium" (see Problem 17.13).

For two spheres, R is replaced by $(1/R_1 + 1/R_2)^{-1}$ in all the above equations.

Equations (17.47)–(17.49) for the adhesion forces are independent of the meniscus radius r_1 so that it is of interest to establish below what radius, relative vapor pressure or

[13]Although this has never been rigorously proved to the author.

RH, these equations break down—that is, when does γ_{SV} become γ_S? McFarlane and Tabor (1950) verified that the adhesion force between glass spheres and a flat glass surface in close to saturated vapors of water, glycerol, decane, octane, alcohol, benzene, and aniline are all given by $F = 4\pi R\gamma_L \cos\theta$ to within a few percentage points. Fisher and Israelachvili (1981) measured the adhesion forces between curved mica surfaces in various vapors such as cyclohexane and benzene and found that $F = 4\pi R\gamma_L \cos\theta$ is already valid once the relative vapor pressures exceed 0.1–0.2, corresponding to meniscus radii of only ~0.5 nm—that is, about the size of the molecules. However, for water, a larger radius of ~2 nm appears to be needed before Eq. (17.47) is satisfied (Christenson, 1988b; Hirz et al., 1992). These results support the analysis in Sect. 17.3 that for molecules that interact via a simple Lennard-Jones (attractive van der Waals) pair-potential, their bulk surface energy is already manifest at very small curvatures.

Since real particle surfaces are often rough their adhesion in vapor is not always given by Eq. (17.47) or (17.49). For example, the adhesion of dry sand particles is very small, and even when slightly moist the adhesion is not much different since the condensed water is only bridging small asperities (Figure 17.20a). However, once r_K exceeds the asperity size but is still less than the particle radius R (Figure 17.20b), the adhesion force attains its full strength of $F = 4\pi R\gamma_L \cos\theta$ as found by McFarlane and Tabor (1950). However, when r_K exceeds R—that is, when the particles are effectively immersed in excess liquid—the adhesion is often again very low because the capillary term disappears. It is for this reason that one can only build sandcastles with moist sand, but not with dry or completely wet sand (*R.* Pashley, unpublished results).

Capillary condensation also occurs when water condenses from a solvent in which it is only sparingly soluble—for example, from hydrocarbon solvents where the solubility is usually below 100 ppm. In such circumstances the presence of even 20 ppm (i.e., 20–40% of saturation) can lead to a dramatic increase in the adhesion of hydrophilic colloidal particles. Indeed, it has long been known that trace amounts of water can have a dramatic effect on colloidal stability (Bloomquist and Shutt, 1940; Parfitt and Peacock, 1978), and surfactant association (Eicke, 1980) in nonpolar organic solvents. The enhanced agglomeration of metal ores and coal particles in oils by addition of water forms the basis of several industrial separation and extraction processes (Henry et al., 1980). Christenson (1983, 1985b) found that in the presence of small amounts (<100 ppm) of water the adhesion force between mica surfaces in benzene, octane, cyclohexane, and the liquid OMCTS is given by Eq. (17.47) to within 20% with γ_L replaced by the liquid-liquid interfacial energy γ_{12}. The enhanced adhesion in such systems arises because γ_{12} is typically 35–50 mJ m^{-2} (see Table 17.1)—much higher than the solid-liquid interfacial energies in the anhydrous liquids.

Finally, an interesting phenomenon occurs when two hydrophobic particles interact in water. If the contact angle exceeds 90° the above equations predict that a *vapor* cavity should "capillary condense" between the two surfaces, again resulting in a strongly adhesive force determined by the high value of the hydrophobic-water interfacial tension. This effect has been observed by Christenson et al., (1989) and Meyer et al., (2006).

PROBLEMS AND DISCUSSION TOPICS

17.1 In Worked Example 17.9 and Figure 17.21, the force between the two surfaces is given by the sum of the Laplace Pressure and resolved surface tension force. However, when calculating the height of rise h of a liquid in a capillary tube of radius r (Figure 1.3a), one considers either the Laplace Pressure ($2\gamma_L/R = 2\gamma_L/r\cos^{-1}\theta$ acting on area πr^2) *or* the resolved surface tension contribution ($\gamma_L \cos\theta$ acting along the circumference $2\pi r$), but not both. Each of these give the same result, viz. $\rho gh = 2\pi\gamma_L \cos\theta/r$, but only one actually contributes. Resolve this apparent paradox.

17.2* (i) With increasing length D the liquid bridge in Figure 17.21 becomes *mechanically* unstable, becoming unduloid and eventually breaking up into two hemispheres (cf. Figure 1.3c). At what value of D will this occur? (ii) Show that the value of D at which the cylinder becomes *thermodynamically* unstable is smaller than this value, and discuss how these two instabilities manifest themselves in practice. Will this second type of instability lead to one, two, or more hemispheres? Would you expect similar instabilities to occur for a thin liquid film adsorbed on (iii) a cylinder and (iv) a flat surface? [*Answer:* (i) $D = 2\pi R = (4\pi V)^{1/3}$, where V is the (constant) volume of the liquid bridge.[14] (ii) One hemisphere. (iii) Yes.]

17.3 Estimate the local tensile pressure acting normal to a solid surface at the point where a macroscopic liquid droplet of water meets the surface (see Fig. 17.12c). What effects could this have on the surface both at the microscopic and molecular levels? [*Answer:* $\gamma_L/\sigma \approx 50$ mJ m^{-2}/0.5 nm $\approx$ 100 MPa $\approx$ 1,000 atm.]

17.4 Why does the 3D pressure of a gas act to *increase* its volume but the 2D pressure of a liquid surface (the surface tension) acts to *decrease* the area?

17.5 Compounds 1 and 2 are both nonpolar liquids and interact only via van der Waals dispersion forces. The Hamaker constant of 1 is larger than that of 2 ($A_1 > A_2$). A small amount of 1 (the solute) is completely dissolved in 2 (the solvent).

- **(i)** Will the concentration of 1 below the surface of the solution be the same, greater than, or less than the bulk concentration? If there is a difference, estimate the distance range over which the concentration will be affected.
- **(ii)** Will the surface tension of the solution be the same, greater than, or less than the value for the pure solvent 2?
- **(iii)** What if $A_1 < A_2$?
- **(iv)** How do your conclusions relate to the "Gibbs Adsorption isotherm"? [*Answer:* (i) Less than. (ii) Greater than. (iii) Greater than, less than.]

17.6 When gas dissolves in a liquid, does the surface tension increase or decrease? [*Answer:* Decrease.]

[14]This is known as the Raleigh Instability. If you think it is a difficult problem, it probably won't be any consolation to you to know that Joseph Plateau solved it more than 150 years ago, and he was blind.

17.7 The 13-atom cluster of Figure 17.4 has 12 identically coordinated atoms in the 1st layer around the central atom. The second and subsequent layers build up to form quasi-spherical HCP clusters. (i) How many van der Waals "bonds" does each atom in the 1st layer make with its nearest neighbors? (ii) How many unsaturated bonds are there per atom in the 1st layer? (iii) How many bonds does each atom in the 1st layer make with those in the 2nd layer? (iv) What is the total number of bonds between the 1st and 2nd layers? (v) How many atoms form the 2nd layer? (vi) What is the average number of bonds that an atom in the 2nd layer makes with those in the first layer? (vii) Does each atom of the 2nd layer make the same number of bonds with those in the 1st layer? [*Answer:* (i) 5. (ii) 7. (iii) 7. (iv) 42. (v) 84. (vi) $84/42 = 2$. (vii) No. Six bond to 4 atoms, 24 bond to two atoms, and 12 bond to one atom, giving an average of exactly two per atom.[15]]

17.8 A hydrophobic surface on which water makes a 90° contact angle has a small circular area of radius r that is hydrophilic with a contact angle of 0°. A syringe slowly ejects water to the center of the hydrophilic circle. Describe, with sketches, how the contact angle changes as the water volume increases from zero to $\frac{4}{3}\pi r^3$, and then decreases again to zero. Repeat your analysis for a surface where the hydrophobic and hydrophilic areas are interchanged. Ignore gravitational effects.

17.9* A wavy surface has shallow depressions that can be approximated by hemispherical cavities of various radii from $r = 5$ mm to $r = \infty$ (planar) as shown in the figure below. (i) A small liquid droplet of volume 2 mm^3 and intrinsic contact angle $\theta_0 = 15°$ (on a planar surface) is placed on the surface. Assuming that the droplet can move about to find its location of lowest energy, without changing its volume, what radius cavity will it settle in? (ii) If the droplet can break up into smaller droplets, each settling in a different cavity, could this lower the total surface energy of the system? (iii) When the surface is exposed to saturated vapor, allowing for condensation to occur, sketch the final equilibrium state of the system. Identify both metastable and stable states. Ignore gravitational effects. [*Answer:* (i) In a cavity of radius $r = 8.2$ mm.]

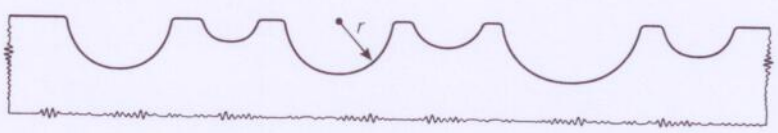

17.10 Derive Eq. (17.45) from the variation of the total surface energy of the system W with distance D, $F = -dW/dD$, assuming constant liquid volume V and small ϕ in Figure 17.20c.

[15]It is interesting to note that the 13-atom cluster exposes six 4-bond and eight 3-bond adsorption sites (see Figure 17.4), yet none of the 3-bond sites end up being occupied in the complete 55-atom cluster.

17.11* Derive Eq. (17.45a) by differentiating the total energy of the system with respect to D for the case of constant chemical potential of the liquid and vapor molecules—that is, assuming thermodynamic equilibrium with the vapor reservoir, so that $r_1 = r_K$ at all separations D. [*Hint:* Since evaporation or condensation must occur as D changes, the free energy associated with this must be included in your energy balance (as a PdV term).]

17.12 The rough surface shown below is exposed to saturated vapor of a liquid that subtends a small contact angle ($\theta \approx 10^\circ$) on the surface. Draw the different stages of capillary condensation from the initial condensate to the final thermodynamic equilibrium configuration of the liquid-vapor interface, noting the mechanically stable, unstable and metastable states on the way. Repeat for when a liquid droplet is placed on the surface (note that the final equilibrium state should be the same). Repeat both of the above for a liquid of contact angle $\theta = 90^\circ$. Ignore gravitational forces. [*Hint:* Consider the Laplace pressure driving the meniscus to always move (by condensation or evaporation) in the concave direction.]

17.13 Water condenses at the junction of two spheres (glass marbles) of radius 1 cm. The contact angle is zero at both surfaces, the RH is 0.9 (90%), and the temperature is 20°C. What is the adhesion force in the case where (i) $\gamma_{SL} = 20$ mJ m^{-2} and (ii) $\gamma_{SL} = 0$, and there is a hard-wall repulsive hydration force at $D = 2.0$ nm? [*Answer to (ii)*: 3.7×10^{-3} N (~0.37 gm).]

17.14 For a microscopic solid sphere, would you expect its (i) density and (ii) boiling point to be larger or smaller than the bulk material?

17.15 A sphere having a density greater than water is carefully placed on a water surface where it is seen to float. Its contact angle with water is 90°. Sketch the geometry of the water surface around the sphere and explain how it is supported given that at the three-phase border all the forces are balanced by the Young equation.

17.16* Two bodies floating on the surface of a denser liquid have contact angles as shown in Figure 17.22. (i) In each case, determine whether the force between the bodies due to surface tension effects is attractive or repulsive. (ii) Sketch the configuration of the bodies in the absence of gravity, where the liquid volume is large and its surface effectively flat. [*Answer to (i):* (a) Attractive, (b) attractive, (c) repulsive.]

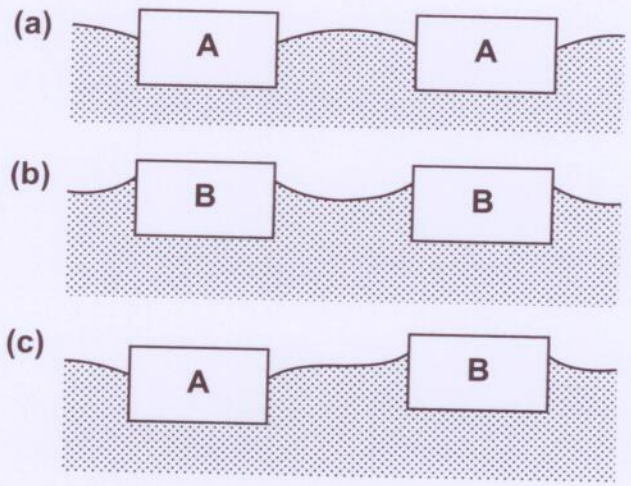

FIGURE 17.22

17.17 Two smooth cylindrical fibers of radii R_1 and R_2 are brought into contact with their axes at an angle α in an atmosphere of water vapor. Show that the adhesive capillary force between them is constant over a large range of relative humidity and is given by

$$F_{ad} = -4\pi\sqrt{R_1R_2}(\gamma_{SL} + \gamma_{LV}\cos\theta)/\sin\alpha. \tag{17.50}$$

Would you expect Eq. (17.50) to overestimate or underestimate the adhesion at (i) low humidities (RH < 50%), (ii) high humidities (RH > 99%), and (iii) small fiber radii (R < 1 μm). What happens when $\alpha = 0°$?

17.18 Prove that for two dissimilar particles—say, two spheres—if one has a contact angle θ the other must have a contact angle less than $(180 - \theta)$ for the capillary force between them to be attractive. What occurs in practice if the capillary force is predicted to be repulsive?

17.19* Two plane parallel surfaces or spheres as in Figure 17.23 are connected by a liquid bridge that is axially symmetric around the vertical z axis. The bridge is in thermodynamic equilibrium with the surrounding saturated vapor (RH = 100%). Show that the profile of the liquid-vapor interface is a catenary described by $r(z) = r_0 \cos h(z/r_0) = r_0(e^{+z/r_0} + e^{-z/r_0})/2$, where r_0 is the radius of the neck at its

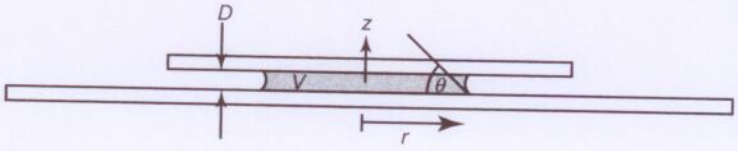

FIGURE 17.23

narrowest point (r_2 in Figure 17.20c). For two plane parallel surfaces (or $r_2 \ll R$) show that the equilibrium force-law $F(D)$ is

$$F(D) = -\pi D\gamma_L/\text{arctan h}(\cos\theta), \tag{17.51}$$

where θ is the contact angle. What does it mean that the force is infinite when $\theta = 90°$?

17.20 Why does the capillary force contribution to the total adhesion force between two rough surfaces often increase and then decrease as the RH increases from 0 to saturation (RH = 100%)?

17.21 A flat surface is brought down onto the flat end of a vertical elastic cylindrical pillar of length L and unit cross-sectional area, to which it adheres with surface energy W. The pillar is attached to a rigid substrate at its lower end. The flat surface is now retracted until the pillar detaches from it when it has stretched by ΔL. If the size of the molecules and effective range of the adhesion forces is σ, (i) what is the force on the surface (and pillar) at the moment of detachment, and (ii) how much energy has been expended by the surface to bring about the separation? If your answer to (ii) is greater than W, where has the excess energy gone to?

17.22 An assembly of nonadhering spheres in a square lattice, with 6-nearest neighbors per sphere, as shown in Figure 17.24, is subjected to a mean compressive pressure P. If K is the bulk elastic modulus of the material of the spheres (i) what is the effective modulus of the "granular material," defined by K_{eff} = stress/strain = $P/(\Delta L/L)$, and (ii) what is the maximum pressure $p_{\max}$ experienced by the spheres—that is, at their points of contact with each other? If the particles are made of glass ($K = 50$ GPa), what is the maximum pressure actually felt by the particles when the mean applied pressure is $P = 1$ GPa? What do your results

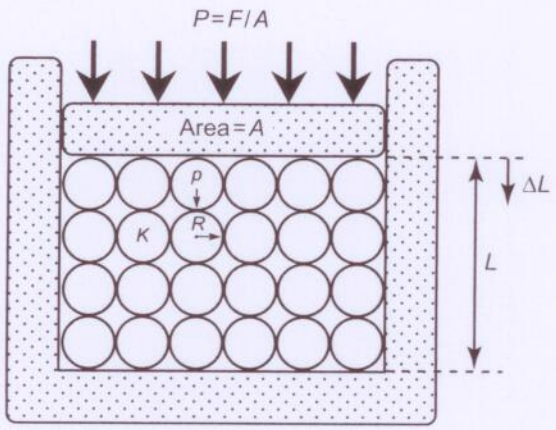

FIGURE 17.24

imply for how one thinks about the "elasticity" and yield stress of granular materials on compression? [*Answer:* (i) For this (Herzian) geometry, ΔL is not a linear function of the load F. Thus, K_{eff} is not a constant even when the spheres themselves deform elastically. (ii) $p_{\max} = 6K^{2/3}P^{1/3}/\pi^{5/3} = 0.9K^{2/3}P^{1/3} = 12$ GPa (12 times the applied pressure).]

17.23* A 6-sided right-angled cuboid crystal has sides of length a, b, and c in the x, y, and z directions, and the three pairs of faces have surface energies γ_a, γ_b, and γ_c, respectively. Show that the lowest total surface energy of a crystal, assumed to be of fixed volume $V = abc$, is when all six faces have the same surface energy—that is, $\gamma_a bc = \gamma_b ac = \gamma_c ab$.[16]

17.24 Give possible reasons for each of the following observations and how you could establish experimentally which ones are responsible.

- **(i)** The adhesion force increases with the *time* the surfaces are in contact.
- **(ii)** The adhesion force increases with the *rate* at which the surfaces are pulled apart.
- **(iii)** The adhesion force increases with the *relative humidity.*
- **(iv)** The adhesion force is *lower* in water and salt solutions.
- **(v)** The adhesion force is *higher* in water and salt solutions.

17.25 How would you expect the adhesion energy between two molecularly smooth surfaces to depend on the relative orientation of their surface crystallographic axes ("twist" angles)?

17.26* A glass beaker contains equal volumes of 3 immiscible liquids that have stratified into 3 layers (phases) according to their density, with the heaviest liquid (No. 1) at the bottom and the lightest (No. 3) at the top. Only van der Waals forces are operating, and the Hamaker constants of the liquids and glass are in the order $A_2 > A_3 > A_1 > A_{\text{glass}} > A_{\text{air}}$. (i) Is there a thin film at any of the interfaces? (ii) What will be the disposition of the liquids in zero gravity?

17.27 Referring to Problem 1.2, at what radius will the gravitational pressure and the pressure due to surface tension be the same at the center of a sphere of liquid water? [*Answer:* $R = 10.0$ m.]

17.28 Figure 17.10 shows six possible configurations of a liquid on a solid surface where the contact angle θ is the same for each. Which is the thermodynamically equilibrium configuration when the vapor above the surface is (i) slightly below and (ii) slightly above the saturated vapor pressure?

17.29 A surface contains two small (~5 mm) droplets or lenses of dissimilar liquids A and B that subtend contact angles $\theta_A = 30°$ and $\theta_B = 10°$. When droplet A is moved toward droplet B using a think glass rod, it is seen that droplet B moves away and that it is very difficult to make the droplets coalesce even though the liquids are mutually miscible. Explain this effect. [*Hint:* Consider that all liquids are at least partially volatile, and the possible effects of precursor films (see Fig. 17.6)].

[16] In practice, crystal shapes are determined more by the different rates at which the different faces grow.

17.30 Show that for a solid-liquid interface of the same material, for example, ice and liquid water, we expect $\gamma_{SV} \approx \gamma_{SL} + \gamma_{LV}$, and check whether this is indeed the case for water, and for one other material. [*Hint:* See Antonow's equation.]

17.31 Where is the missing point VI in Figure 17.14, mentioned in the text on the previous page?